Microgravity Application Program / Biotechnology

Mid Term Report for ESA-Project

ESTEC Contract # 14592/00/NL/SH

MAP AO-99-030, CCN 001, CCN 002

"2D and 3D Quantification of Bone Structure and its Changes in Microgravity Condition by Measures of Complexity"

Coordinator:	
Peter Saparin (PS)	Max Planck Institute of Colloids and Interfaces, Germany (MPI)
Wolfgang Gowin (WG)	Project coordinator until 31.07.2004. Independent, Germany
Team Members:	
Jesper Skovhus Thomsen, (JST)	University of Aarhus, Denmark (UoA)
Peter Fratzl (PF)	MPI of Colloids and Interfaces, Germany (MPI)
Richard Weinkamer (RW)	MPI of Colloids and Interfaces, Germany (MPI)
Dieter Felsenberg, (DF)	Campus Benjamin Franklin, Charité, Germany (CBF)
Gisela Beller (GB)	Campus Benjamin Franklin, Charité, Germany (CBF)
Jürgen Kurths (JK)	University Potsdam, Germany (UoP)
Norbert Marwan (NM)	University Potsdam, Germany (UoP)
Hans-Christian Hege (CH)	Zuse Institute, Berlin, Germany (ZIB)
Steffen Prohaska (SP)	Zuse Institute, Berlin, Germany (ZIB)
Bruno Koller (BK)	Scanco Medical AG, Switzerland (Industry)
Christian Asbeck (CA)	Siemens AG, Forchheim, Germany (Industry)
Malte Westerhoff (MW)	Mercury Computer Systems GmbH, Germany (Industry)

November 2004

Table of Content

1. Set-up of the pQCT-Scanner Suitable for Structural Analysis of Bone Images

Our need has been to find a scanner able to examine the structure of proximal tibia below the knee joint. It should have a gantry opening of max. 18 cm. However, such a scanner is presently not available commercially. The machine to our requirements and manufactured currently is the pQCT-scanner XCT-3000 produced by Stratec Medizintechnik GmbH, which has a gantry opening of 28 cm.

The commercial configuration of the XCT-3000 is limited to BMD measurements and macroscopic measurements like endosteal and periosteal circumferences or moments of inertia. Therefore, it was arranged with the manufacturer to produce a machine with an individual adapted configuration that is able to acquire an image with a quality suitable for structural analysis. The machine was ordered in June 2003. By the end of August 2003, it was ready at the factory for the special configuration. Team member Wolfgang Gowin visited the manufacturer where he spent three days changing the hardware and the software set up – together with the Stratec personnel – to fit our requirements. Several sets of images were electronically transferred to Berlin and analyzed by team member Peter Saparin until the best image quality was achieved. The current set up runs at the upper safe limit of the X-ray tube: 0.450 mA.

The pQCT-scanner has been located at the CBF facility since September 1, 2003, see Figure 1. Numerous images were acquired from bone specimens of proximal tibiae and lumbar vertebrae in 2003 and 2004. In-vivo examination of proximal tibiae from test persons started in April 2004. All supportive materials and safety precautions have been applied to the machine in order to scan the proximal tibia on test persons.

Figure 1. The pQCT-scanner allows in-vivo imaging and structural analysis of proximal tibia.

2. Computer Hardware Set-up at MPI, UoP, and ZIB

In the continuation proposal, we identified the computer hardware that was suited to our purpose: an external disk-array, a RAM extension as well as a new NAS Server.

The project workstation HP Visualize J6000 has been moved to the Department of Biomaterials, Max Planck Institute of Colloids and Interfaces, as the project coordinator Peter Saparin received new position at this institute. The initial configuration of the HP Visualize J6000 workstation was: dual RISC processors PA-8600 at 552 MHz, 4 GB of RAM, and 72 GB of disk space on 2 internal disks.

However, due to the dramatic increase of data volume related to the processing of the vertebral bodies and newly acquired images from bone specimens as well as in-vivo examinations, the workstation had to be upgraded. Required hardware was purchased as it was planned in the continuation proposal. The RAM was extended to 16 GB, and two external hard disks with a total capacity of 180 GB were attached to the system in September 2003.

In order to make it possible for the partner UoP to visualize and develop quantification approaches for 3D datasets, a 64-bit Itanium2 workstation with a high performance graphics board was purchased. The workstation HP ZX6000 is equipped with two 1.3 GHz Itanium2 processors, 4 GB RAM, an internal 73 GB SCSI hard drive, and a NVIDIA Quadro4 980XGL graphics card. The proposed Itanium2 workstation was ordered at the end of October 2003, but because of supply difficulties by HP, the machine was not delivered until mid of January 2004. The required operating system RedHat Linux was delivered in February 2004. The system has been configured and the Amira environment has been installed. Since the end of February 2004, the workstation has been heavily used and serves the needs of the project.

The project's data server – Dual Pentium 1 GHz with 160 GB of disk storage – was moved from CBF to ZIB in September 2003. Additionally, a Network Attached Storage (NAS) with 1 TB disk space (750 GB when used as RAID 5) was installed and is available to all cooperation partners. The acquired 2D and 3D image data is stored on this server. Data is also manually archived in ZIB's tape library.

3. Collection and Imaging of Bone Specimens and Patients

3.1.1 Collection of additional specimens

In addition to the bone specimens harvested during the phase I of the project (2001–2002), 31 sets of specimens consisting of the third (L3) and fourth (L4) lumbar vertebrae, a proximal tibia and a calcaneus (or the whole foot) of the same side were collected at the Department of Anatomy, Charité, Campus Mitte, as a result of collaboration with the head of the department Prof. G. Bogusch.. Each single set of bone samples was harvested form one body donor (subject). All specimens were stored in formalin solution. All bones underwent an air extracting procedure (see earlier reports) to remove artifact generating air bubbles inside the bones. Thereafter, the specimens were packed into plastic bags filled with formalin and stored at approximately 3°C.

3.1.2 Conventional X-ray examination of the specimens

All specimens underwent a conventional X-ray examination in order to detect pathologic changes of the bones.

Since we planned to perform all further investigations on whole sets of specimens, we excluded all sets with fractured third or fourth lumbar vertebral bodies (7 cases) or with other pathologic changes (0 cases as evaluated by x-ray).

3.1.3 pQCT imaging of specimens

In order to establish the procedures of biomechanical testing at whole vertebral bodies of L3 (section 7.2) and histomorphometry of L4 (section 7.3) we rescanned five L3 and L4 vertebral bodies collected for the first phase of the project with the new XCT 3000 scanner as a pilot study.

Thereafter, the remaining 24 newly collected L3 vertebral bodies were pQCT scanned and the images were visually evaluated. After this evaluation, four more cases showing pathological changes were excluded. However, one specimen with osteolytic and one with osteoblastic changes remained included in the material. Consequently, the material comprised sets of bones from 20 individuals. The fourth lumbar vertebral bodies and the proximal tibiae were also pQCT scanned. The scans at the proximal tibiae were performed 17 mm below the articular joint, which is the same location as we used for obtaining trabecular bone biopsies in the first phase of the project.

All scans of vertebral bodies and proximal tibia specimens were performed with the same predefined scan parameters. We performed one 2 mm thick axial slice (tomography) trough the middle of the vertebral body. The aim of pQCT and CT imaging was to mach the scanned location of both methods (both with 2 mm thick slices) as good as possible. When pQCT imaging was done before CT imaging, the pQCT imaging was set as our reference that we tried to find again by the CT examination. In the beginning of the investigations, only one scout view was preformed as preparation for the pQCT scan. However, it turned out that this approach caused massive problems with adjusting the positioning of the specimens for the CT imaging and consumed unpredictable amounts of time with repetitions of whole series of CT examinations. Finally, we decided to repeat all previously performed pQCTs scans with two perpendicular scout views. We were then able to match the positioning of the specimens for pQCT and CT imaging to an acceptable degree.

3.2 pQCT imaging of test subjects

After some minor modifications of the equipment, we were able to perform pQCT of 5 test subjects. The positioning of the subjects lasts about 30 to 90 minutes. In order to receive high-resolution pQCT-images it is necessary to perform three scans at 20 mm/s. This causes the performance of a pQCT scan itself to last approximately 20 minutes. Therefore, even if the test subjects are fixed in the scanner, in order to reduce moving artefacts, it is very difficult to obtain images that are free from artefacts due to movements.

3.3 CT imaging : definition and optimization of acquisition parameters. of specimens. Vertebral body and proximal tibia examination in patients with new Siemens CT-technology

Since we had no previous experience with high-resolution spiral CT imaging, we had to start at a very low level. The recommended scan parameter we received from Siemens AG turned out to be unusable. We were able to acquire high-resolution images, but the noise level was approximately ten times higher than in the single slice images provided by Siemens Somatom Plus scanner, which was used during the first phase of the project. In addition, it turned out that the selected device Siemens Somatom Sensation 16 would not enable us to perform axial slice images at the lumbar vertebrae of test subjects as the gantry of the device cannot be tilted in spiral mode. Fortunately, we had the opportunity to move our experiments to a Siemens Somatom Sensation 4 helical CT-scanner that is also located at CBF.

After several adjustments and test scans with different kernels, collimations and rotation times, and with different modes (spiral CT and single slice technique) we were able to establish a first set up of scan parameters suitable for high resolution images of a quality needed for evaluation by the structural parameters.

We scanned the 5 L3 and 5 L4 vertebral bodies collected during the first phase of the project for the biomechanical pilot study that was to be performed at the UoA (by Jesper Skovhus Thomsen) (section 7.2).

Furthermore, the 20 L3 and 20 L4 vertebral bodies of the new collected sets of specimen were scanned also scanned.

All these 50 vertebral bodies were fully scanned in spiral CT mode (axial volumetric acquisition of the entire vertebral body). Furthermore, sequences of axial single slice images were obtained through the middle region of the vertebral body (approximately 1 cm high). Spiral CT delivered volumetric sequences of high-resolution images with 1 and 2 mm slice thicknesses. Single slice CT delivered high-resolution images with a 4 mm slice thickness. As described above, the matching of the positioning of the specimens was very difficult. A difference of only 1° in the positioning of the specimens resulted in serious problems in matching the acquired vertebral trabecular patterns. However, using dual scout scans as described for the pQCT scanning resolved this problem.

We scanned 20 proximal tibiae in single slice technique with slice thicknesses of 1, 2 and 4 mm at the same location as used for the pQCT scans.

In order to transfer the scan parameter from specimen to *in vivo* measurements on test subjects, we started by scanning a body equivalent object, the Euopean Spine Phantom (ESP). As noise doubles for each 8 cm of object diameter, the noise was increased to a level approximately three times that of the noise level of the images of the specimens. Additional test scans with higher mAs lead to reduced noise. However, we found that even with the increased noise level the image quality was good enough to perform structural analysis, and we therefore decided to keep the defined 120 mAs level so as to minimized the effective radiation dose.

Several additional experiments were carried out from January 2004 to July 2004 in order to verify our acquisition parameters and the sensitivity of the structural evaluation to the positioning of the specimens. Firstly, the specimens were positioned at different tilt angles. Secondly, several new kernels were tested with a series of variant collimations and rotation times.

Thirdly, different possibilities of performance of reconstructions (4 mm reconstructions with narrow collimation of the spiral CT were reconstructed out of 1 mm slices, multi planar reconstructions were used, 1 and 2 mm reconstructions were done out of 4 mm single slice images, etc) were evaluated.

Finally, we performed 3 *in vivo* scans of L3 vertebral bodies as well as 4 *in vivo* scans of proximal tibiae. The scans of proximal tibiae were location matched with the pQCT scans performed on the same subjects, see Section 4.

Since the Siemens Somatom Sensation 4 helical CT-scanner that we have used is not going to be manufactured in the future, we transferred our acquisition parameters and defined some new settings for the Siemens Somatom Emotion 6 scanner. In this way, we gained knowledge on how to transfer the imaging and the structural evaluation technique to a different type CT-machine.

Further examinations of patients and *bone structural alterations during follow-up measurements* are planed to take place at the CBF as an additional part of an ADOC study. However, the request for the ethics committee to examine six patients in the follow up study has been submitted, but we have yet to receive a final decision on our application.

3.4 µCT-examination of the vertebral bodies

Ten vertebral bodies, five L3 and five L4 vertebrae, collected during the first phase of the project were used as a pilot study to establish the procedures of vertebral histomorphometry and biomechanical testing (see Sections 7.3 and 7.2). The specimens were sent to Scanco Medical for µCT-imaging before the biomechanical tests, and the L3 vertebral bodies were scanned again after the biomechanical compression tests performed at UoA.

After the procedures for vertebral histomorphometry and biomechanical testing were established, a newly collected set of 20 L3 vertebral bodies and 20 L4 vertebral bodies were sent to Scanco Medical AG for µCT scanning. All these specimens have been scanned to the date of report. The 3D datasets from all scanned vertebral bodies have been received and are stored on the project central data server at ZIB.

The 3D imaging of vertebral bodies was performed on the Scanco µCT 80 micro-CT machine. This µCT-scanner has a microfocus x-ray-source with a spot size of 5 µm, and its characteristics are: 50–70 kVp and 8W (160 µA). The detector has 2048 × 128 elements and 48 µm pitch. The machine provides a resolution of 10 µm nominal, and 16 µm for 10% MTF at 20 mm Ø. The image matrix can be set to 512 × 512, 1024 × 1024, or 2048 × 2048 pixels. The analyzed specimen can be up to 75 mm in diameter and up to 125 mm long.

The vertebral data sets were acquired with a voxel size of 37 µm (0.0371 mm × 0.0371 mm × 0.0370 mm). This corresponds to an average number of slices of approximately 800 and an acquisition time of approximately 2.75 hour.

3.5 Efforts to identify ultrasound partner

The project coordinator has established contact with three potential cooperation partners from Latvia, Poland, and France which are specialized in ultrasound research of bone material to take over the role of Texon Technologies. In addition, recently Roger Binot (ESTEC) has provided contact details of a French ultrasound scientist; a communication channel has not been yet established. Therefore, the project team needs to discuss with ESA whether they have any experience working with any of the suggested potential partners; and whether ESA

has any administrative preferences or limitation when working with the institutions from Latvia and Poland. The details are provided in the Report on the Project Mid-Term Meeting, November 2, 2004.

4. Manual Bone Biopsy Technique

The procedure to take bone biopsies at different skeletal locations is established, and the tools to perform the task are evaluated. In summary, the bone biopsy set SDI (Surgical Diamond Instruments) is recommended for long bone biopsies out of larger trabecular bones, whereas the Rochester Bone Biopsy set fulfills its purpose for iliac crest biopsies.

The SDI set includes a compressed air driven drilling machine, a hollow diamond drill bit (hollow milling cutter), extractors, and a special drill bit release. For histomorphometric purposes the hollow diamond drill bit should have a diameter of 7 mm, larger bits are available. SDI is very useful for large bones. The instruments allow going deep into the trabecular bone without any difficulties. The main problems arise from unclean bits and wobbling leads of the drilling machine. Therefore, ultrasound cleaning of the bits is essential as well as a steady hand for the drilling procedure. The bone dust particles are extremely small and are pressed into the biopsy by only 0.5 mm. The procedure with SDI is very safe on the trabecular bone. We did not observe mini-fractures or any other manipulation of the trabecular network in our biopsies.

The Rochester Bone Biopsy set has the option to be driven by a drilling machine. The teeth are much sharper and better designed, so that the cutter works unequally smoother than the Meunier Threphine which is the most often used biopsy set. The Rochester set is very good for taking bone biopsies from the iliac crest region (specimens or patients). The bone dust is minimal; however the potential to break trabeculae artificially exists when the cutter changes the direction slightly during cutting. Therefore, long biopsies taken from large trabecular areas are not the main task for this set. In conclusion, this set can be recommended for iliac crest bone biopsies, in particular, from patients.

5. Evaluation of Bone Structure from 2D Images Acquired from Patients

The algorithms for in-vivo 2D examinations in pQCT have been adapted. Algorithms for the in-vivo QCT-examination of the lumbar spine and proximal tibia (Bonus: proximal tibia CT-examinations had not been planned) have been adapted as well. Massive changes were required due to the new CT-scanner from Siemens. All modules for the analysis software of patient examination on CT- and pQCT-scanners are designed, tested, and implemented. The method of quantifying bone structure with measures of complexity is transferable to patient examinations at different skeletal sites.

The new pQCT-scanner for patient examinations has been delivered to the facility at CBF. We were able to adapt the algorithms already established for density and structural assessments of bones quickly to the new technical parameters given by the new scanner. The scanner is used to scan human bone specimens as well as in vivo proximal tibiae 15 to 20 mm below the knee of a patient.

The new 4-line helical CT-scanner Siemens Sensation is available at the CBF. Difficulties appeared immediately due to the reconstruction algorithms used for routine set-ups of the

scanner. These algorithms are built and optimized for visual interpretation of images. Most reconstruction algorithms are therefore edge-enhanced. However, the quantification procedure of bone trabeculae requires non-enhanced reconstruction algorithms. Our industrial partner Siemens provided solutions to suit our needs. The new reconstruction algorithms were embedded into a special set-up protocol for lumbar spine examinations. We tested the algorithm and found an improvement in image quality (noise reduction and signal enhancement) compared with the previous set-up of the Somatom Plus S CT-scanner.

The adaptation of our analysis algorithms were experimentally found and are tested and implemented now. This part of the adaptation procedure seemed to be relatively simple due to the improved image quality.

In addition to the original proposal and CCN 001, we decided to perform CT-examination of the proximal tibia. Due to the improved image quality of the new helical CT-scanner, we are now able to explore the potential of using the CT-procedure for examination of the proximal tibia. Our preliminary results show that this approach makes the proposed procedure of bone status assessment for the space-flying personnel easier, faster, and it requires only one scanner. The original proposal required two scanners: a CT-scanner for lumbar spine examination and a pQCT-scanner for the proximal tibia examination.

The appropriate modules for the software performing the analysis of 2D patients' images derived from helical CT-scanner and pQCT-scanners have been designed. They are tested and implemented. First results from in-vivo examination of bone structure of healthy test persons are obtained and reported below.

5.1 Quantification of Bone structure from Vertebral and Tibial CT- and pQCT-Images Acquired In-Vivo: First Results

The approach to quantify bone structure with the measures of complexity is being adapted to two different kinds of CT-machines capable of obtaining bone images in-vivo:

- Whole-body CT scanner Siemens Sensation 4 Volume Zoom;
- Peripheral quantitative computer tomography (pQCT) scanner XCT3000, Stratec Medizintechnik GmbH, Pforzheim, Germany.

The devices provide CT-images of distinctive parameters and resolution, but, most importantly, the radiation exposures for a patient are very different. The dose obtained by a patient during the pQCT investigation is 10 times less than the one received during CT-imaging of the lumbar spine region. In addition, the price of the pQCT machine is only a fraction of the cost of the whole-body CT-scanner.

Five **healthy volunteers** (no known bone diseases), age range 31 to 52 years, four males and one female, were selected for the pilot study. CT-images of vertebra L3, CT-images of proximal tibia, and pQCT-images of the proximal tibia were acquired from every person (Figure 2). Slice location in L3 vertebrae: center of vertebral body in the transaxial direction.

The proximal tibia images were acquired 17 mm below the knee joint. Slice thickness of vertebral CT-images is 4 mm, while slice thickness of tibial pQCT images is 2 mm. In order to compare the bones' structure from the tibial CT-images with the structure of the lumbar vertebrae from CT-images, one set of tibial CT-images has been obtained with a slice thickness of 4 mm. Next, in order to perform quantitative comparison of the CT- and pQCT-images of proximal tibiae, another set of tibial CT-images with slice thickness of 2 mm has been acquired. The entire set of the CT- and pQCT-images obtained in-vivo from one test person is

shown in Figure 2. To the date of the report four test persons were examined on the CT-machine and five volunteers were examined with the pQCT-scanner.

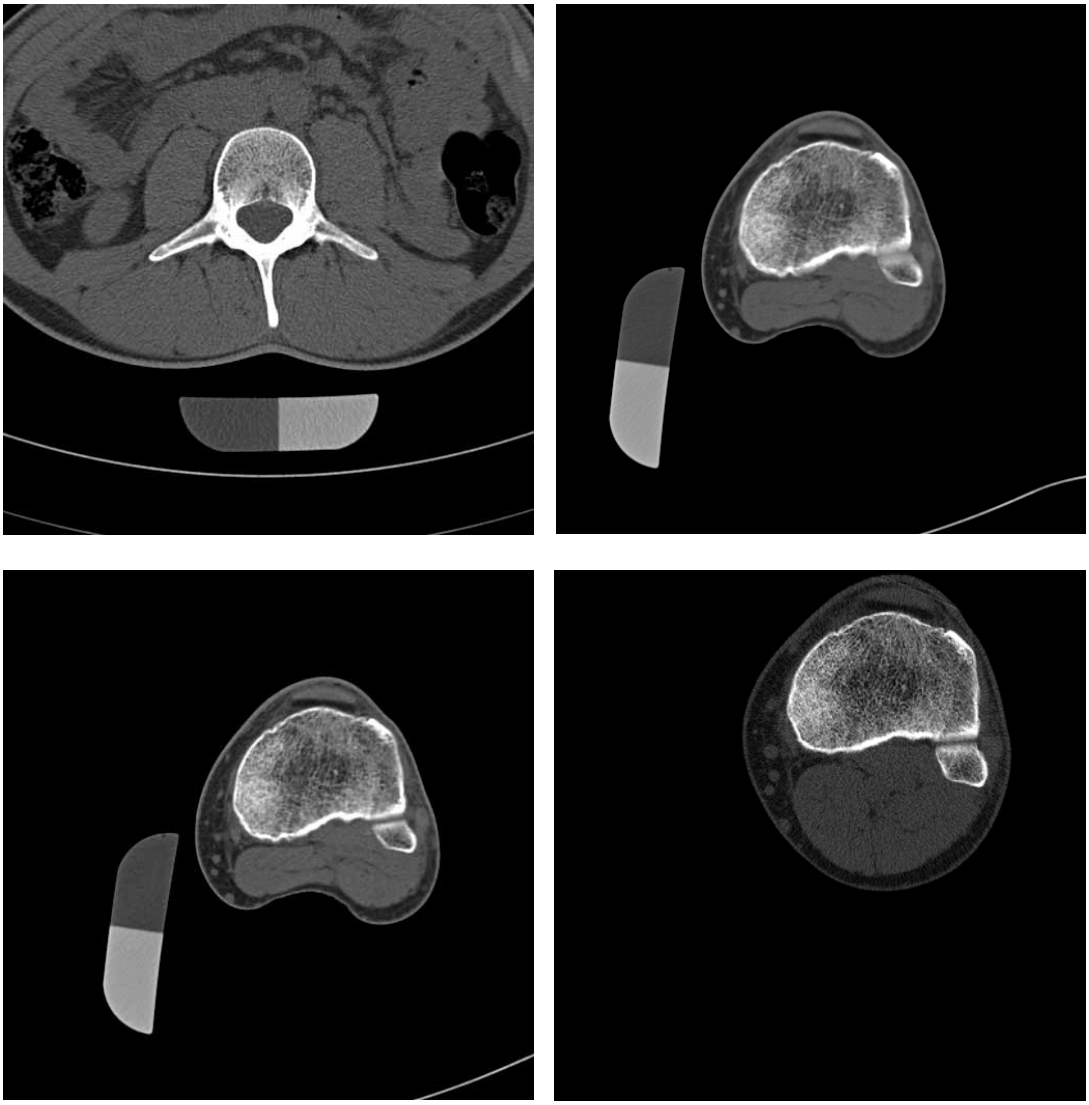

Figure 2. A set of CT- and pQCT-images obtained in-vivo from the same test person. *Top left:* CT-image of lumbar vertebral L3, slice thickness 4 mm. *Top right:* CT-image of proximal tibia, slice thickness 4 mm. *Bottom left:* CT-image of proximal tibia, slice thickness 2 mm. *Bottom right:* pQCT-slice through the same region of proximal tibia, slice thickness 2 mm.

The linear **signal-to-noise ratio** SNR in different regions of different images has been estimated. The SNR in the vertebral CT-images (3.2 in trabecular bone area) is much lower than in the tibial CT- images (9.8 and 8.8 in trabecular bone area of 4 mm and 2 mm thick slices correspondingly) due to the large amount of soft and connective tissue surrounding the vertebrae. The lowest SNR = 2.4 was found in the trabecular bone area of the pQCT images. The pQCT-scanner is a low radiation device, and, as it is known, smaller radiation dose means higher level of noise distortion.

Analysis of **complexity of vertebral bone architecture** revealed the differences in structural organization of normal bones. The two younger individuals B and C have higher values of their vertebral BMDs; the complexity of their vertebral architectures is 2.6 times higher than the complexity found in the older individual A with a lower BMD. The Maximal L-block,

which assesses the area between the trabeculae, has almost the same low value for the two younger volunteers B and C. This measure is 3.3 times higher for test person A. Despite the large differences in complexity, the TNI difference between all three test persons is less than 37%. In general, no discordance in the behaviour of the structural measures and BMD was found in the analysis of vertebral CT-images.

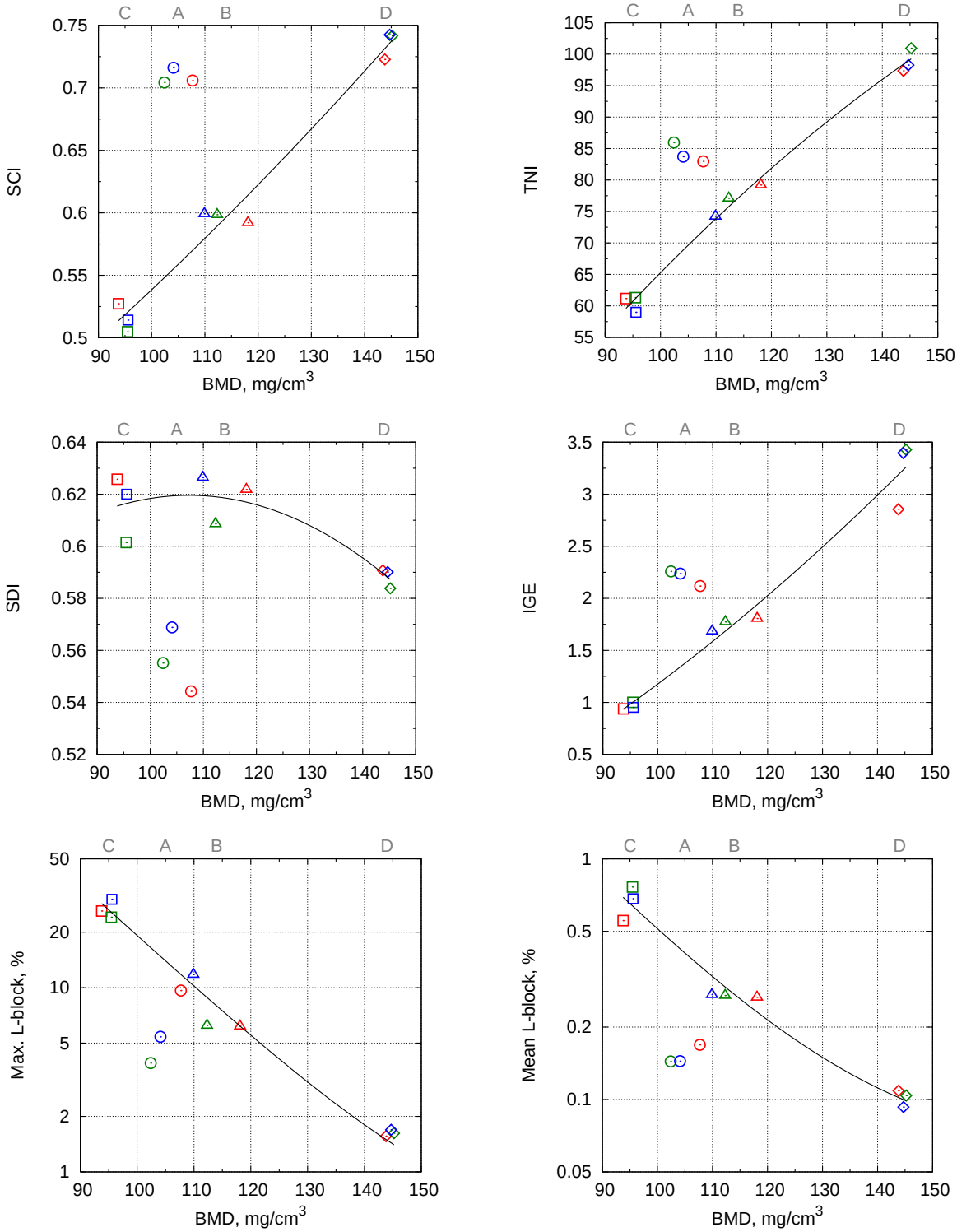

Figure 3. Diagrams bone structure – bone density for trabecular bone of proximal tibia obtained from CT-images. Color depicts image parameters as follows (slice thickness / pixel size): 2 mm / 445 µm, 4 mm / 445 µm, 4 mm / 390 µm. The different test persons are presented by the symbols of different shape. The test person IDs are shown at the top of every plot.

The six **bone structure–bone density diagrams for** trabecular bone of **proximal tibia obtained from the CT-images** shown in Figure 3 illustrate the relation between the density and the architecture of trabecular bone assessed by six different measures of complexity. The results are obtained from CT-images of proximal tibia, with a slice thickness of 2 mm (pixel size 445 µm) and 4 mm (pixel size 445 µm and 390 µm). Analysis of these diagrams reveals very interesting differences in the behaviour of the BMD and the structural measures. For person A, despite a low BMD value, the complexity of the bone architecture is almost as high as the structural complexity of bone D, which has the highest BMD. The SCI is 30% higher than expected for a bone with such a low BMD value. The difference in structural composition of this bone is captured and quantified by all others structural measures: TNI is 20% higher, IGE is 65% higher, and L-block measures are 1.5–3 times lower than expected for the bone of such a low BMD. The degree of disorder (SDI) within the architecture is even smaller than what is found in the bones with higher BMD values. In proximal tibiae the results of the entire bone evaluation confirm all findings we made by analyzing the trabecular bone alone. In particular, despite the low BMD value in the proximal tibia of individual A, the complexity of its architecture is maximal and its degree of disorder is minimal among all analyzed subjects when the entire bone slice is analyzed.

Comparing the **BMD derived from the CT- and the pQCT tibial images** we found that the BMD calculated from the pQCT image is always lower than the BMD estimated from the corresponding CT-image. The differences are 4%–11% despite the fact that both machines were cross-calibrated using the Siemens calibration phantom and the European Forearm Phantom EFP. The cross-calibration results confirmed that the BMD values obtained from the homogeneous areas of the test phantoms are similar for both pQCT and CT-images. Thus, the reason for BMD differences is the way in which the trabecular structure is depicted in the pQCT and CT-images. In order to quantify the differences in bone images acquired by the CT- and pQCT-scanners we calculate the apparent bone volume to total volume ratio BV/TV. The differences in apparent BV/TV reach 20–30%. Bone elements appear much thinner in the pQCT images than in the CT-images. The BMD is calculated as an average over the bone area. The smaller the number of pixels occupied by the bone material is, the smaller the resulting BMD value will be. These differences in presentation of bone elements in CT- and pQCT-images must be taken into account when comparing both density and structural parameters from the images acquired by the different CT-machines.

As we found the SNR is rather low in tibial pQCT-images acquired in-vivo. In order to perform **analysis of the bone structure from pQCT tibial images acquired in-vivo**, it is necessary to separate the bone architecture from the underlying noise fluctuations. Thus, a noise reduction algorithm must be applied. As we found in the first phase of the project, an effective noise reduction algorithm for pQCT-images is Adaptive Smoothing Based on Local Statistics (SLS). After the SLS noise reduction is applied, the SNR in pQCT images increases more than two times. All results reported below are obtained after the application of this noise reduction algorithm.

Five healthy volunteers have been measured with the pQCT to the date of this report. The results of their bone status evaluation are shown on diagrams bone structure–bone density as presented in Figure 4. Among all analyzed pQCT-images the proximal tibia of a newly included test subject E is characterized by having the highest values of its architectural complexity SCI, the trabecular network index TNI, and the BMD. However, despite the highest BMD value, its structure is ranked as second only by the SDI, the IGE, and the maximal L-block.

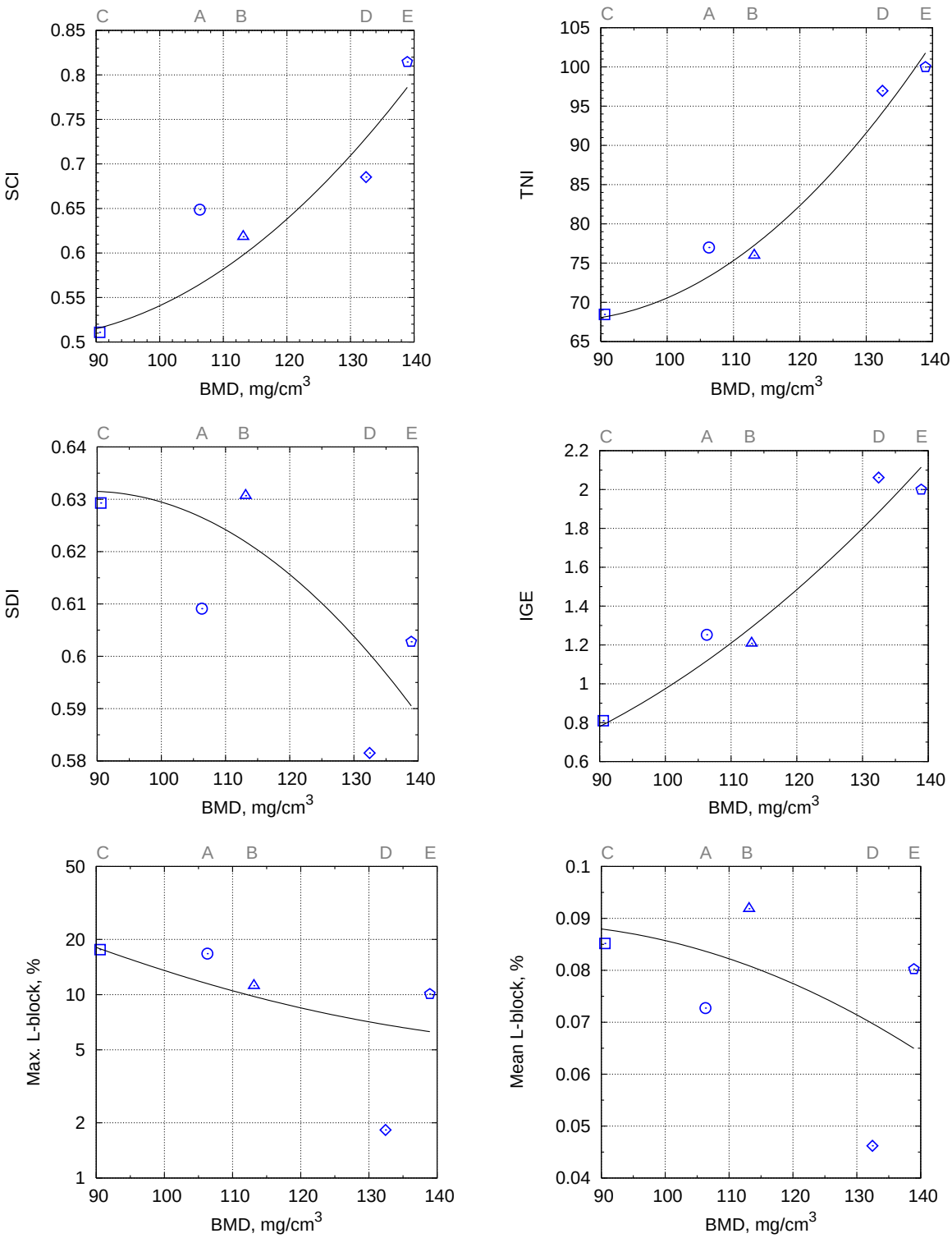

Figure 4. Measures of complexity plotted on the diagrams bone structure – bone density for trabecular bone of proximal tibia obtained from pQCT-images. Slice thickness is 2 mm, pixel size is 250 µm. The different test persons are presented by the symbols of different shape. The test person IDs are shown at the top of every plot.

It is important that the evaluation of tibial pQCT images confirms all the conclusion we made in regards of the special structural properties of the proximal tibia of test person A based in CT-images. Despite the lower BMD value, the structure of this bone is assessed by the structural measures as being close to normal. The pQCT-based structural measures provide the same ranking of the bone architectures as the measures obtained from CT-images. Only L-block based measures derived from pQCT- and CT-image rank the bones with intermediate BMD in a slightly different way. As these measures quantify the organization of inter-

trabecular regions, they are the measures that are most affected by the differences in depiction of bone elements by CT- and pQCT-scanners.

The conclusion from this preliminary study (work in progress) can be summarized as follows:

- Thus, we found that the evaluation of the pQCT tibial images confirms the discordance in the ranking of bones by their status provided by the structural measures and by the BMD.
- The developed technique is able to quantify the bone structure from CT- and pQCT-images taken in-vivo.
- The structural composition of bones images obtained from healthy individuals can be differentiated.
- The evaluation of vertebrae and tibiae results in different ranking of bones by the structural measures and the BMD as well.
- The evaluation of tibial CT-images of different slice thicknesses and pQCT-images provides similar conclusion about bone structure in different individuals.
- The structural measures of complexity and the BMD provide different information about the bone and rank analyzed tibia by their status in a different way.

5.2 Recommendation for bone status assessment of space-flying personnel

Our recommendation for bone status assessment of space-flying personnel is an examination procedure that requires a non-invasive radiological procedure before space flight and after return to Earth. CT-images of the lumbar vertebra L3 and CT- or pQCT-images of the proximal tibia about 17 mm below the knee joint of one leg shall be acquired. The image analysis program includes bone mineral density measurements and the quantification of the architectural composition of the bone regions by measures of complexity. The image acquisition requires keeping certain acquisition parameters constant. The method is standardized.

The examination of the axial skeleton at the lumbar spine by QCT is already the “gold standard” for bone density assessment. The additional evaluation of the structural composition of the very same images omits additional radiation exposure. By evaluating the density and the structural composition we achieve the utmost outcome of this non-invasive procedure. It provides a complete morphological status of the axial skeleton.

The lower extremities experience the highest degree of unloading during exposure to microgravity. It is therefore essential to quantify the process of changes in the legs. The proximal tibia has a very rich trabecular network. It is similar in its behavior to the vertebral body. The proximal tibia is easily accessible. Both, the density as well as the structural composition will be evaluated at this site.

By comparing the outcome of the axial skeletal examination with the peripheral skeletal examination, we will be able to determine any discordance in changes due to microgravity exposure. This is going to be the essential point to design and initiate individual countermeasures.

6. 3D Quantification and Visualization of Bone Structure

6.1 3D measures of complexity based on the approach developed to analyze 2D CT-images

The techniques of symbolic encoding in conjunction with symbolic dynamics have been used to extend our set of 2D measures of complexity into a set of 3D measures of complexity. Based on the knowledge gained in the project during the work with 3D CT-images, we selected a twofold approach to work with 3D datasets. Firstly, we developed two measures that use raw or binarized μCT datasets: 3D Normalized Entropy (S_{norm}) and Structure Complexity Index based on the 3D distribution of local spatial ratios of bone volume to total volume BV/TV_{loc} ($SCI(BV/TV_{loc})$). Secondly, we developed three measures that use symbol-encoded datasets: Structure Complexity Index, SCI3D; Surface Complexity Index; Surface Index of Global Ensemble, SurfIGE.

The 3D symbolic encoding procedure has changed substantially in comparison with the 2D symbolic encoding procedure. The purpose of the symbol-encoding procedure is to reduce the amount of information in a 3D μCT dataset to its essential structural composition. Our initial intention was to use the same symbolic encoding procedure as applied to the 2D CT-images. This method was based on an alphabet of five different symbols: three static and two dynamic symbols. However, we found that the edge definition and the distribution of attenuation within the trabeculae of the 3D μCT datasets was not as sharp and well defined as those obtained by a high-resolution 2D CT. Under these circumstances, the five-symbol-encoding method is too sensitive.

We then tested an encoding based on the binarization of the 3D data set. In this encoding, the structure is represented only by two types of symbols: B, for bone and M, for marrow. We found that such an encoding, while adequate for quantification of extremely robust properties of bone architecture, could be further improved by the introduction of an additional symbol that represents the information about the bone surface i.e. the transition from bone to marrow.

As for 2D bone image encoding, it is important to use a mixture of both static and dynamic encoding to obtain more information about the analyzed structure. The dynamic symbol in the 3D encoding is the surface symbol derived from a combination of geometrical and attenuation information. Thus, the modified symbol-encoding procedure for the μCT data is based on an alphabet of three different symbols: M, for marrow voxel; I, for internal bone voxel; and S, for surface bone voxel. The first two symbols are static, while the last, S, is dynamic. Bone "surface" S is a one-voxel-thick layer of bone voxels which are lying at the boundary between two tissues: bone and marrow.

Due to the changes in the symbolic encoding, the set of 2D complexity measures had to be modified thoroughly in order to deal with 3D objects.

In 3D, all voxels representing marrow are connected with each other [15]. Therefore, 2D L-block based measures become obsolete. The smaller number of symbols available for encoding requires a redefinition of SDI and TNI for 3D purposes. Since a direct generalization or a transfer of these measures into a 3D quantification is impossible, two other complexity measures were introduced to assess spatial aspects of the bone architecture. 3D Normalized Entropy of the geometrical locations and the Structure Complexity Index based on 3D distribution of local spatial ratios of bone volume to total volume BV/TV_{loc}, see below, which are two new measures that do not require of the symbolic encoding.

Thus, based on the generalization of our 2D technique, the following set of five most appropriate complexity measures to quantify 3D architecture is found:

- **3D Normalized Entropy of geometrical locations of bone tissue, S_{norm},** is an expression of the distribution of material in space. It is basically a general geometrical measure that supplements a simple material measure such as BMD.
- **Structure Complexity Index based on 3D distribution of local spatial ratios of bone volume to total volume BV/TV_{loc} , $SCI(BV/TV_{loc})$,** is the entropy of the local BV/TV distributions and quantifies local inhomogeneities of the material distribution in space. It utilizes local bone fraction BV/TV inspired by the histomorphometry to construct a 3D measure of complexity.
- **Structure Complexity Index, SCI3D,** is similar to the SCI of 2D measurements. It is the entropy of the probabilities of the local ratio of bone voxels (internal and surface) to marrow voxels. It is an expression of the complexity of the structural composition on a local basis, indicating that it also quantifies inhomogeneities of material distributions.
- **Surface Complexity Index, SurfCI,** is the entropy of the distribution of local surface voxels in relation to the accompanying bone voxels. This measure evaluates the spatial distribution of increasing/decreasing surfaces on a local basis.
- **Surface Index of Global Ensemble, SurfIGE,** is the entropy of the distribution of all surface voxels in relation to bone voxels. This measure expresses the relationship of surface geometry to bone material in general.

In order to evaluate the ability of the developed measures for quantification of 3D structural complexity in bone, the proposed measures were compared in detail against the "gold standard" of trabecular bone assessment: histomorphometry. Each of the histomorphometric parameters describes a different aspect of the organization of the bone material. In order to study the correlation between the different histomorphometric parameters and the measures of complexity, they were compared pair wise by using the Spearman's rank-order correlation coefficient r_s. The correlation between two measures was considered to be good if $r_s>0.6$. A high correlation coefficient with a particular histomorphometric parameter indicates that the corresponding information is included in the considered measure of complexity.

Good correlation with the histomorphometric parameters quantifying the distribution of trabeculae, Tb.N, Tb.Sp, and to CD (r_s = 0.61, -0.76 and 0.7) confirms that the Normalized Entropy is capable of assessing the bone geometrical composition in 3D.

Another 3D structural parameter, SurfIGE correlates well with Tb.Th, Nd.Tm, and TBPf with correlation coefficient r_s = -0.75, -0.72, and 0.73 respectively.

The complexity measures SCI3D correlates to six and SurfCI correlates to four histomorphometric measures simultaneously. SCI3D correlates: to the amount of bone material expressed by 3D BV/TV (r_s = 0.94), to the geometry of trabecular bone network assessed by Tb.Th, Tb.N, Tb.Sp, Nd/Tm, $V^*_{m.space}$ (r_s= 0.7, 0.64, -0.8, 0.76), to the distribution of material in 3D space quantified by the Normalized Entropy S_{norm}, and TBPf (r_s = 0.9,-0.79) as well as to the other complexity measures SurfCI and SurfIGE.

SurfCI includes information about the amount of bone material (quantified by BV/TV, r_s = 0.8), the geometry of the construction (for Tb.N, Tb.Sp, and $V^*_{m.space}$ r_s = 0.66, -0.76, -0.61), and the connectivity of the trabeculae (expressed by CD, r_s =0.7). SurfCI values are also in excellent agreement (r_s > 0.91) with two other 3D measures of complexity: SCI3D and SCI(BV/TV).

The only histomorphometric measure of trabecular bone structure that has a firm foundation in topology is connectivity density (CD), and it is therefore one of the most important histomorphometric measures. Among *all* analyzed measures, including other parameters based on histomorphometry, the best correlation to CD is obtained by the complexity measures: SurfCI (r_s = 0.7) and 3D Normalized Entropy of geometrical locations (r_s= 0.64). In addition, this is an indication that the other new 3D measures of complexity quantify different aspects of the 3D structure than those quantified with the connectivity density.

The correlation between the complexity measures and the histomorphometric measures confirms that the new proposed 3D measures of complexity are able to quantify the spatial architecture of the trabecular bone. These measures combine and assess different kinds of information and quantify the bone architecture in a holistic way.

A scientific paper has been written and is accepted for publication in Acta Astronautica.

6.2 Newly Developed 3D Measures of Complexity for Assessment of Spatial Bone Architecture

New approaches are developed on an ongoing basis in our efforts to introduce innovative 3D quantification parameters for bone architecture. Several new 3D measures of complexity have been introduced by using different approaches originating in fractal analysis, spatial correlation, recurrence analysis as well as geometrical and topological analysis. These measures were applied to the 3D µCT data acquired from proximal tibia biopsies. In order to validate the proposed measures, we compared the results with the histomorphometric measures of the biopsies.

6.2.1 Lacunarity and Morisita's index

Lacunarity is a measure, which is related to gapiness and translational invariance. This measure also enables the recognition of characteristic length scales of the studied object. In this project, we extended the original definition for 2D objects to a definition for 3D objects and applied this measure for the first time to 3D data. (Here we are using a normalized version of lacunarity, which avoids bias effects due to different box sizes.) High lacunarity values represent less translational invariance compared with low lacunarity values. A similar measure, the Morisita's index, which was developed in several studies of eco-systems, was also used. However, this measure is closely related to lacunarity and the results are very similar. Therefore, it is not discussed in more detail here.

The lacunarity for the µCT data of proximal tibia is stronger correlated with connectivity density than with bone volume fration (Figure 5). Thus, bones with high or low bone volume fraction may have similar translational invariance, whereas bone with high connectivity density has low translational invariance and bone with low connectivity density has high translational invariance. Therefore, the lacunarity provides further information about the trabecular structures, which cannot be revealed with bone volume fraction alone.

6.2.2 Moran's and Geary's index

From a 2D image analysis, we adopted a spatial auto-correlation test, the *Moran's index*, to 3D. This index quantifies the spatial correlation between pairs of contiguous neighbours. Its values vary between -1 and +1 — if the autocorrelation is high, the index will tend toward -1; if autocorrelation is numerically high but negative, the index will tend toward +1, and if not

correlated, the index will be zero. The *Geary's index* is based on a rather similar definition and is highly correlated with the Moran's index; its values typically range between 0 and 2, where 0 indicates negative spatial autocorrelation, 2 positive spatial autocorrelation and 1 no autocorrelation. It was the first time that these two indices were used for 3D bone analysis.

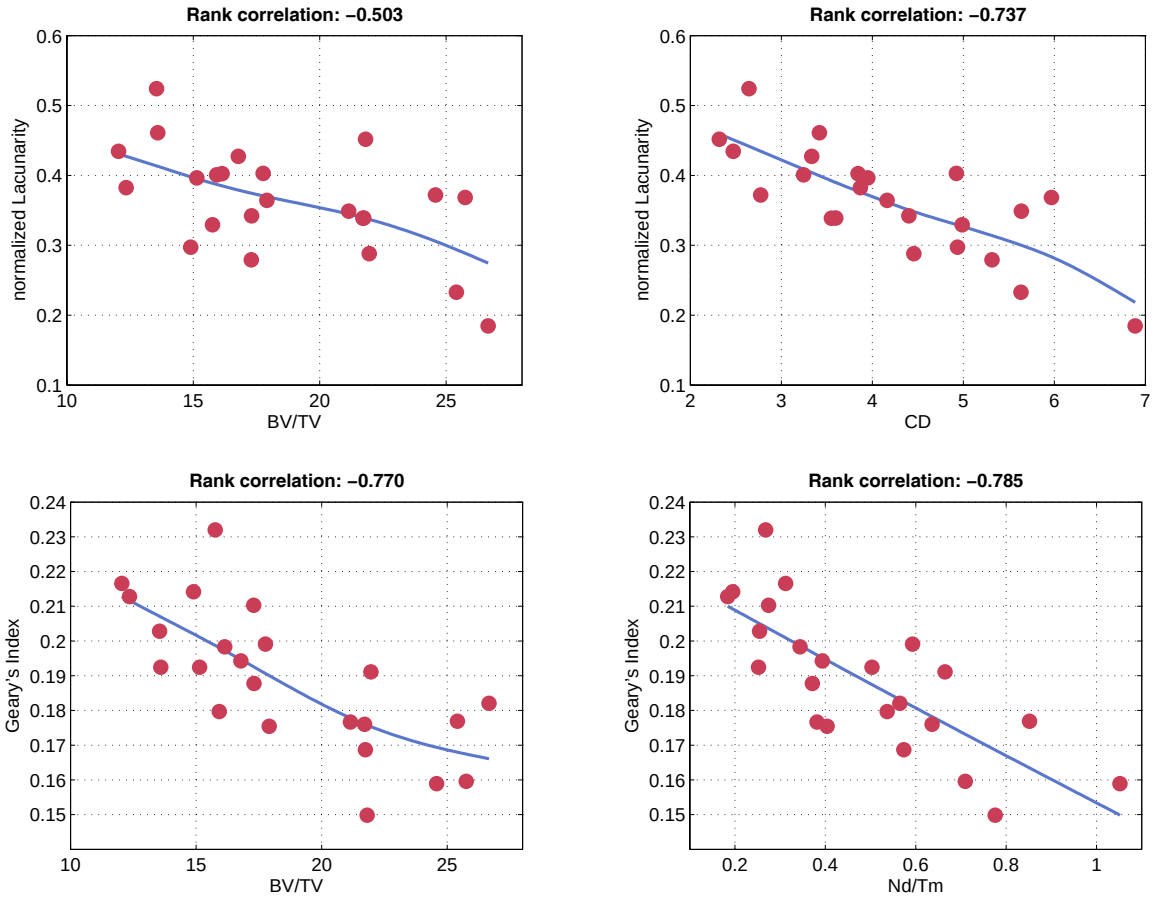

Figure 5. Normalized lacunarity and Geary's index versus histomorphometric measures bone volume fraction BV/TV [%] and node terminus ratio Nd/Tm for proximal tibia biopsies.

The application of these measures to the µCT data of the proximal tibia reveals a high anti-correlation of neighbouring voxels for bone with high bone volume fraction (Figure 5). For decreasing bone density, the spatial auto-correlation decreases. This observation indicates that the surface of the bone becomes less complex during bone loss. Furthermore, from this analysis we found that Moran's index and Geary's index are highly related with 2D histomorphometric measures that quantify structural aspects of the trabecular network, such as node-terminus ratio (Nd/Tm) and trabecular bone pattern factor (TBPf). In the first part of this project, it was shown, in the same proximal tibial biopsies, that TBPf is very closely related to the structural modelling index (SMI), which quantifies the balance between rod-like and plate-like trabeculae. Therefore, this indicates that Moran's and Geary's index also quantify the balance between rod-like and plate-like trabeculae.

6.2.3 Shape index and marching cubes based measures

The shape index is a measure, which uses the effect that the surface of three-dimensional objects of same volume depends on their shape; e.g., a sphere has the smallest surface for a given volume. Based on this relation, we introduced the new 3D measures *averaged shape index ASHI* and *shape complexity SHC*. The marching cubes algorithm is used to construct a 3D surface from a set of voxels. From this algorithmic approach of estimating the surface and

volume of the bone, we have derived further measures, the *marching cubes entropy index MCE* and the *marching cubes complexity MCC*. All these measures are related with the local shape of the studied structures.

The application of these measures to data from proximal tibia and a subsequent comparison with the corresponding histomorphometric measures shows clearly that these new introduced measures provide information about the trabecular shape, the complexity of the microarchitecture, and the connectivity. The averaged shape index increases for decreasing bone, from which we infer that the number of concave structures decreases and plate-like structures change to rod-like structures (rod-like structures have a larger shape index, Figures 6 and 7). This finding is to some extend confirmed by the anti-correlation of this measure with the trabecular thickness (Tb.Th). The shape complexity reveals a similar result; but more

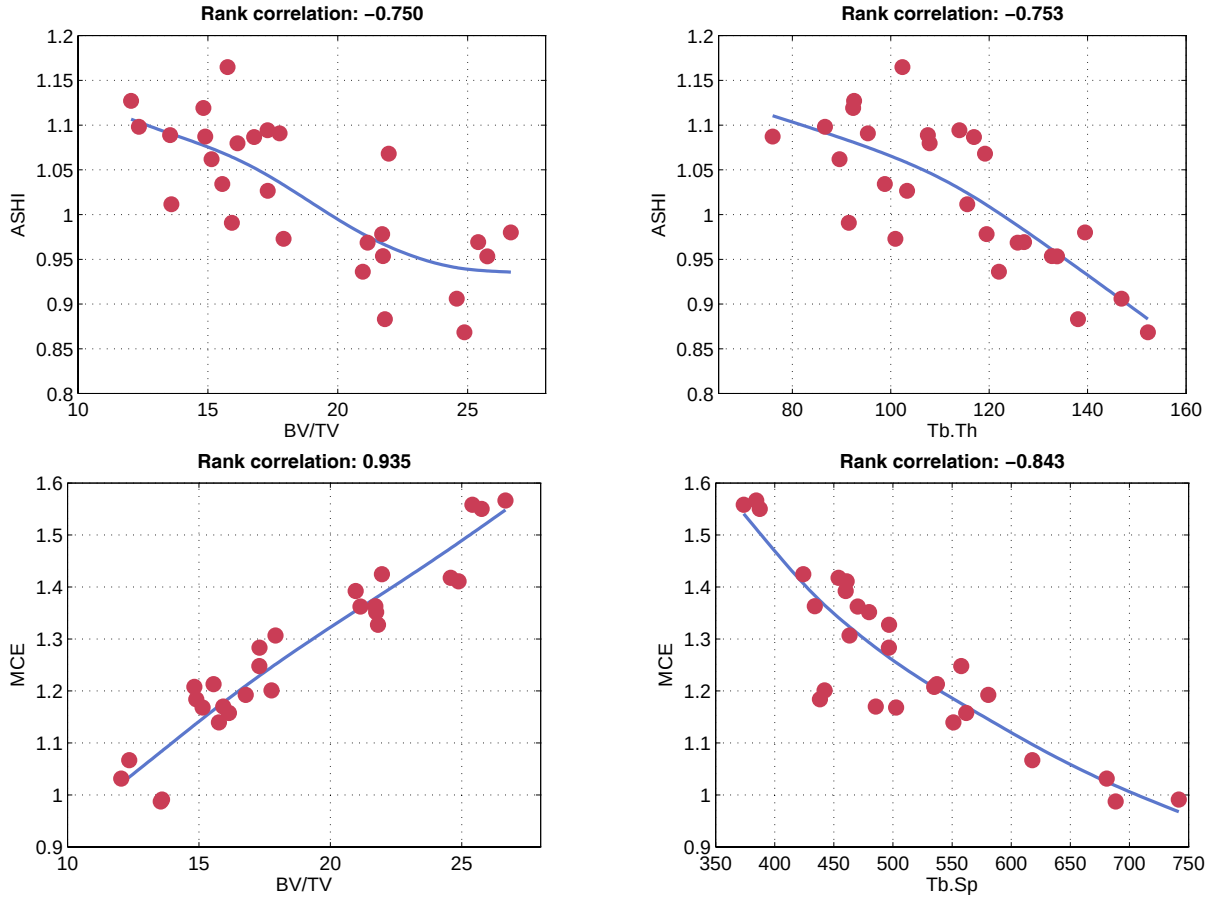

Figure 7. Measures of complexity averaged shape index ASHI, marching cubes entropy index MCE and mean curvature H versus bone volume fraction BV/TV [%] and other histomorphometric measures Tb.Th [µm], Tb.Sp [µm], as well as SMI. The comparison of the measures of complexity with histomorphometric measures confirms the ability of these measures to assess the structural changes.

importantly, it is well correlated with the structural model index (SMI).

The marching cubes based measures reveal a strong decrease during bone loss (Figure 7). This confirms the previous findings that the complexity of bone surface decreases with bone loss. Moreover, these measures show relations with those histomorphometric measures which depend on connectivity and geometrical properties, like node-terminus ratio (Nd/Tm), trabecular bone pattern factor (TBPf), trabecular number (Tb.N), trabecular separation (Tb.Sp), and structural model index (SMI).

6.2.4. Curvatures and curvature based measures

Based on the principal curvatures (mean curvature H and total curvature K), we introduced the *curvatures mutual information* and the *curvatures Kullback-Leibler distance*. Both measures quantify the differences in the joint-distributions of the principal curvatures.

We found generally a positive mean curvature value for all the proximal tibial biopsies. This means that on average convex structures dominate over concave structures. During bone loss the mean curvature increases (Figure 7). Similar to the marching cubes based measures, the mean curvature is related with those histomorphometric measures, which depend on connectivity and geometrical properties. In contrast, the total curvature is uncorrelated with bone volume fraction and most of the histomorphometric measures. It shows only a relationship with the connectivity density. This suggests that the total curvature measure contains additional information about the structural changes to that already available from bone volume fraction. However, the curvatures mutual information and the curvatures Kullback–Leibler distance did not reveal as clear results as expected. Nevertheless, they showed a relation with bone volume fraction and with other histomorphometric measures.

6.2.5 Recurrence plot approach

Starting from the recurrence quantification analysis for one-dimensional time series, we developed a higher dimensional extension of recurrence quantification. This approach quantifies the number and size of recurrent structures in 3D images. However, this method is still under development. The preliminary results were not as good as expected. Moreover, at this time the computational power needed for this method cannot be fulfilled with the currently available computers.

6.2.6 Integration of the developed approaches into Amira system

Amira software was designed as a highly interactive software system for visual data analysis. The tools for 3D evaluation of bone structure with the developed measures of complexity are programmed and implemented as Amira modules or Amira script objects. Within the Amira framework, a complete working environment has been established integrating 3D image visualization and analysis, 3D measurements and assessment, as well as simulation procedures for controlled bone structure alteration (see Figure 8). Script objects are available in order to batch-process a set of 3D data.

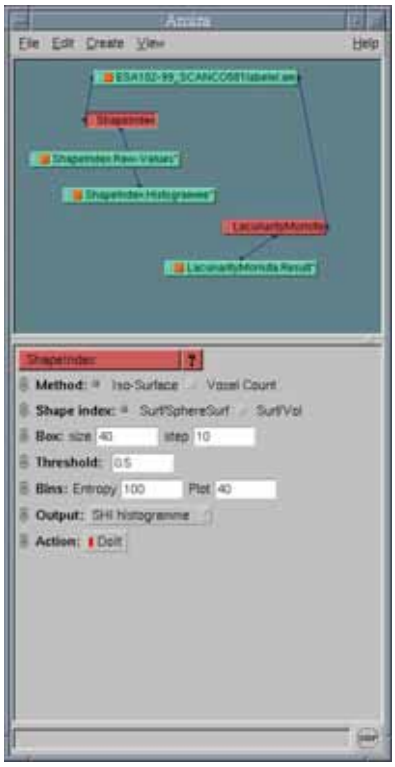

Figure 8. Implementation of modules to calculate Shape Index, Lacunarity and Morisita Index within the Amira framework.

6.3 Further Development and Expansion of 3D Visualization Tools in Amira

Interactivity in Amira is mainly achieved by utilizing local graphics hardware and main memory. The original design assumes that data sets are always completely loaded into main memory and can be indexed using a 32-bit integer. Under this assumption, data sets are limited to a size of 2 GB. In order to use Amira for visualizing data sets larger than this limit, new software interfaces to 3D image data were developed and integrated into Amira. The interfaces provide access to sub-volumes of a volume larger than main memory that is only stored on disk (out-of-core processing). In a second step, a suitable implementation of this concept was needed.

In order to fulfill this goal, the HDF5 file format and library (http://hdf.ncsa.uiuc.edu/HDF5/) are used. Micro-CT scans of vertebral bodies were converted to the HDF5 file format, and can now be efficiently visualized using Amira. Basic visualization algorithms – orthogonal slicing and volume rendering – are directly available. Other methods require the user to manually choose a resolution and sub-volume, which is then loaded. All standard Amira visualization modules are then applicable to the sub-volume.

The amount of acquired image data makes it unfeasible to replicate the data at every cooperation partner. The data sets are only stored centrally at ZIB. To allow other partners to access the data easily, remote data access based on Globus (http://www.globus.org/) was integrated into Amira. All visualization algorithms described above are transparently available when accessing the centrally stored data sets. An article describing the overall system was published at IEEE Visualization [Prohaska, 2004].

6.3.1 Visualization of huge vertebral data sets with Amira

Some applications of the system can be highlighted as follows. It was successfully used to compare data acquired by a whole-body clinical CT scanner and data acquired using µCT (Figure 9). This procedure allows selecting a volume of interest in the 3D data, which matches the location of the 2D whole-body CT slice.

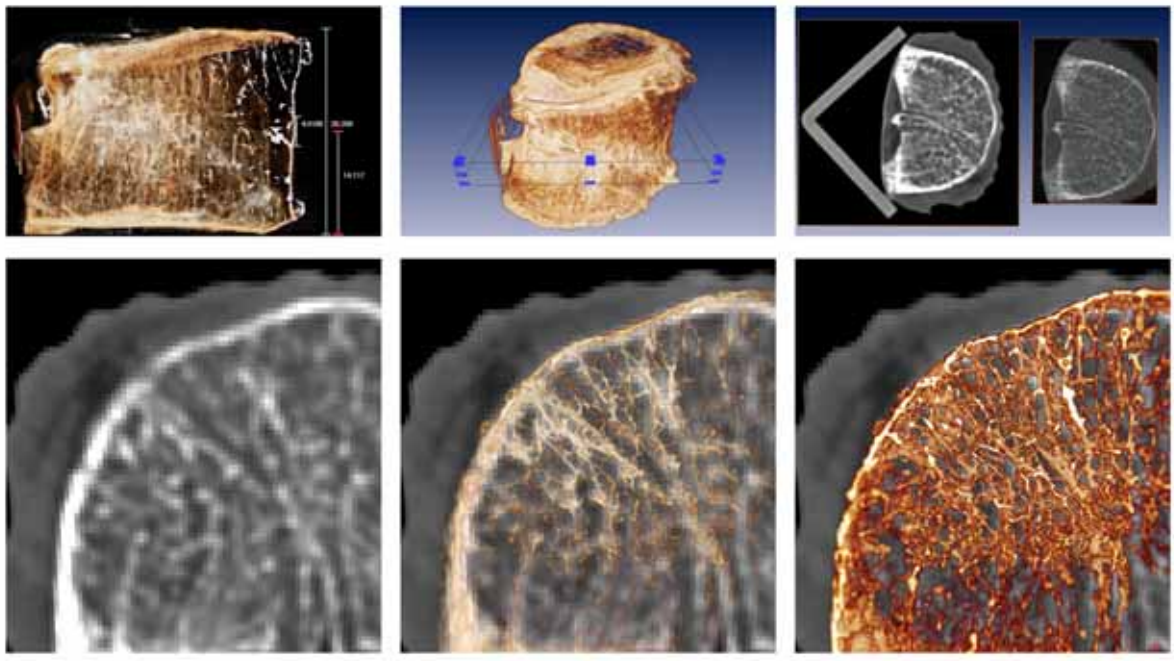

Figure 9: Comparison of image data acquired with a whole-body CT scanner and data acquired using a µCT. Top row: A central 4 mm thick slice is selected and averaged in z direction. The 4 mm slice from the standard CT scanner is visually matched. Left: Orthogonal side view with measurement tools (length in mm). Center: A sub-volume is selected using an interactive dragger. Right: The slice from the µCT (right) is compared to the slice from the CT scanner. Bottom row: After matching the slice location, the internal bone structure can be directly compared with the CT slice. Left: CT slice. Center: CT slice overlaid with transparent volume rendering. Right: Volume rendering showing the rich trabecular structure – only part of it at full resolution.

6.3.2 Comparison of the vertebral bone structure before and after mechanical testing

In order to investigate how the mechanical testing influences the trabecular bone structure the entire vertebral bodies were µCT-scanned before and after mechanical testing (section 7.2). In Figure 10 a sub-volume of a vertebral body is compared before and after failure-load testing. Buckled trabeculae are searched in the volume by visually inspecting sub-volumes. Though this is a tedious, manual task, it is possible to find buckled trabeculae. However, in order to perform quantitative analyses this task has to be automated.

Figure 10 illustrates how a single trabecula has buckled during compression testing, whereas the rest of the trabecular bone network in the sub-volume appears largely intact. The right-most image in Figure 10 shows the location of the sub-volume in the vertebral body. It is worth noting that the buckled trabecula shown in Figure 10 represents an example of *plastic* deformation. During compression the vertebrae undergoes both *plastic* and *elastic* deformation. Plastic deformation occurs at high strain values and result in the non-linear part of the stress-strain curve (see section 7.3), whereas elastic deformation gives a linear contribution to the stress-strain curve (Hook's Law).

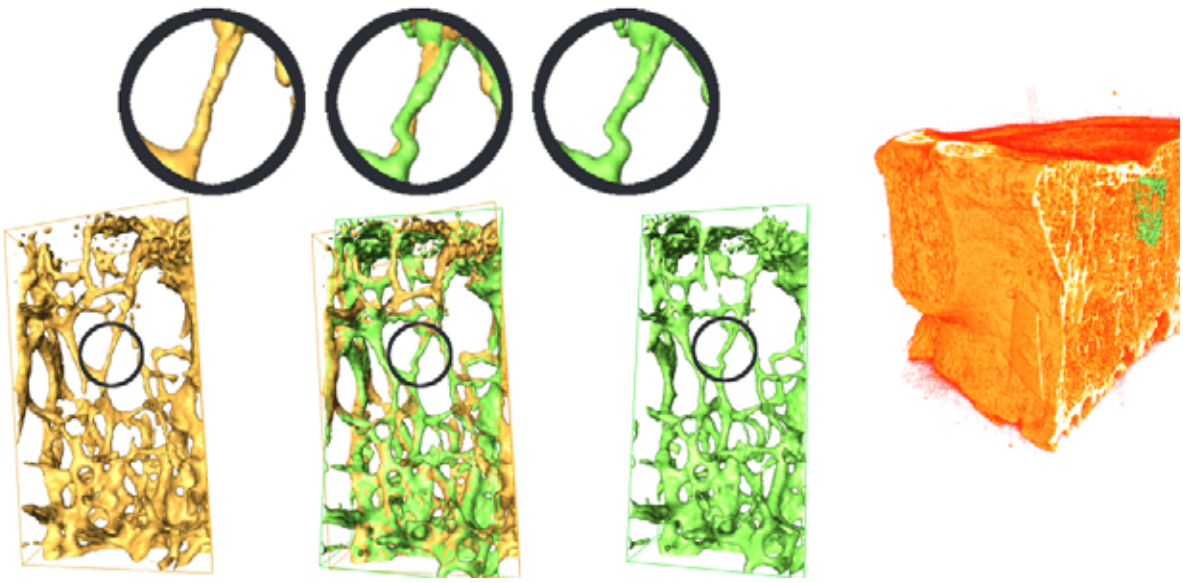

Figure 10: Visual search for buckled trabeculae after failure load testing. Displayed at the right is an overview of the analyzed vertebral structure. The green volume shows the location of the sub-volume, which is magnified on the left. It is located in the mid-height frontal part of the vertebral body near the top cortical shell. The sub-volume before failure load testing is displayed in yellow. The sub-volume after failure load testing is displayed in green. Three close-up views at the top highlight the part of the sub-volume where one of the trabeculae have buckled during the compression. By visual inspection it is possible to find some differences in trabecular configuration before and after compression.

This task is currently under investigation and must therefore be considered as "work in progress". However, our initial experiments show that it is possible to identify individual trabeculae that have buckled during mechanical testing to failure with the current set-up. It is also clear from Figure 10 that the vertebrae as such do not undergo large changes during compression testing. However, the resolution of the µCT scans limits the ability to identify tiny fracture lines in an otherwise unchanged trabecular network. Nevertheless, our initial findings show results similar to those recently reported by Nazarian and Müller [14]. They mechanically tested a small trabecular bone sampled during µCT scanning. However, their technique is limited to small trabecular bone samples, whereas we are able to investigate entire human vertebral bodies. Therefore, we are, able to exactly pinpoint the location of local structural

changes in the vertebral body (as Figure 10 illustrates), which is a unique feature of the present investigation.

7. Histomorphometrical Examinations and Biomechanical Tests

7.1 Histomorphometry on iliac crest bone biopsies from a 370-day-long bed rest study

Through Professor Boris Vladimirovich Morukov the team gained access to iliac crest bone sections from a 370-days-long bed rest study conducted at the Institute for Biomedical Problems (IMBP) in Moscow during the late 1980ies. The iliac bone biopsies were embedded, sectioned, and stained in St Etienne, France by Professor Laurence Vico and co-workers.

This trail is the bed rest experiment with the longest duration ever to be carried out. Consequently, these iliac crest bone biopsies gave the team a unique opportunity to investigate the bone structural changes that takes place during long-term skeletal unloading.

The trail comprised 27–42 years (mean 35.4 years) males which were divided in two study groups, A (n = 4) and B (n = 5), so that the groups were balanced with respect to age, height, and body weight. However, the sections from one of the biopsies from one of the test subjects in group A were mislaid before the team got access to them. Consequently, histomorphometry was available from only 3 of the 4 subjects in group A.

During bed rest, the subjects were placed with a 5° head-down tilt. The head-down tilt (antiorthostatic) bed rest is better able to reproduce the physiological responses due to altered fluid distribution experienced by space flying personnel exposed to microgravity than horizontal bed rest [5,6,7].

The subjects in group A were prophylactic treated orally with the bisphosphonate Xidifon in a dose of 900 mg per day. Concurrent with the bisphosphonate treatment regimen, the subjects in group A underwent an exercise regimen similar to that recommended for prolonged spaceflight [18]. The exercise regimen was comprised of a treadmill and a bicycle ergometer, which were both operated from the horizontal position. The exercise regimen was divided into three 120-day cycles. During each cycle, no exercise took place from day 0 to day 20, whereas exercise was performed for one hour per day from day 21 to day 60 and for two hours per day from day 61 to day 120. However, the final cycle was extended with ten days to a total duration of 130 days. Cylindrical transiliac bone biopsies with a diameter of 8 mm were obtained at the standardized position 2 cm below the iliac crest and 2 cm behind the antero-superior iliac spine [1] before the beginning of the bed rest at the left ileum, and at day 366 at the right ileum.

The subjects in group B did not, at any point during the study, receive any bisphosphonate treatment. Furthermore, the subjects in group B did not perform any exercise in the first 120-day-cycle, whereas they followed the same exercise regimen as the subjects in group A during the last two cycles (i.e. from day 121 to day 370). Transiliac bone biopsies with a diameter of 8 mm were obtained at the left ileum before the beginning of the bed rest, at the right ileum at day 116, and again at the left ileum at day 366.

The biopsies were infiltrated and embedded in methylmethacrylate and four 7-µm-thick non-consecutive sections were cut on a Jung model K microtome for each biopsy. The undecalcified bone sections were stained with modified Goldner trichrome. The stained and mounted

sections were placed directly in an image scanner with an integrated transparency scanning unit (Epson Perfection 3200 Photo, Seiko Epson, Nagano, Japan) and digital images were obtained in a resolution of 2540 dpi (pixel size: 10 µm × 10 µm). The images were interactively edited in order to remove sectioning artifacts and drilling residue and threshold filtered in order to produce black-and-white images.

The computer program that was used for the histomorphometrical analyses is the same as that used in the first phase of the study to analyse proximal tibial biopsies. A detailed description of the program has previously been published [19]. The researcher (JST) was blinded for the group distribution during the histomorphometric measurements in order to obviate measurement bias. Comparison of histomorphometric measures between two time points was performed with a paired samples *t*-test using SPSS version 10.0.

Figure 11 shows the results of the histomorphometric analyses for each test subject. Individual data points are shown with a filled circle. Data points from each test subject have been connected with solid lines, whereas average values for all individuals in the particular group are shown with dashed lines.

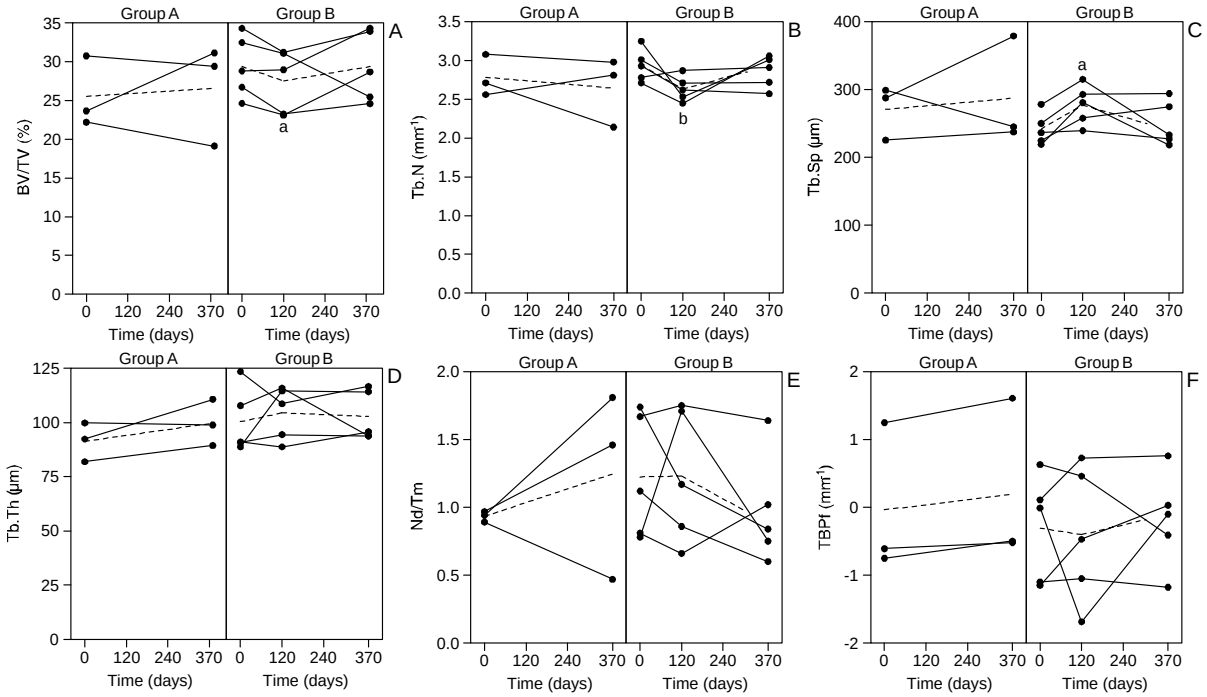

Figure 11 Trabecular bone volume, BV/TV (A); Trabecular number, Tb.N (B); Trabecular separation, Tb.Sp (C); trabecular thickness Tb.Th (D); node terminus ratio, Nd/Tm (E); and trabecular bone pattern factor, TBPf (F) as functions of time for groups A and B. Dashed lines indicate average values for the individuals in the particular group. Key: a: $p < 0.05$ and b: $p < 0.08$. Exact data values are shown in Table 1.

The 120 days of bed rest without countermeasures resulted in a significant ($p = 0.046$) decrease of BV/TV (6.3%) and a significant ($p = 0.020$) increase of Tb.Sp (14.7%). This reduction in trabecular bone density corresponds to a loss of 0.37% per week. Furthermore, a decrease of Tb.N (10.2%) was also found, but this was significant at the 0.08 level only. No other significant changes were found for the histomorphometric measures between any of the time points in either of the study groups. Both $V^{*}_{\mathrm{b.space}}$ (20.9%) and Tb.Th (4.1%) were increased after 120 days of bed rest without countermeasures, indicating a larger average trabecular thickness after immobilization. However, neither of these changes was statistically significant. Figure 11 E and F illustrate that the changes of the two 2D bone structural measures Nd/Tm and TBPf exhibit very complex behaviour at the different time points for the subjects in group B.

	Group A (n = 3)		Group B (n = 5)		
Variables	baseline	day 366	baseline	day 116	day 366
BV/TV (%)	25.5 ± 4.6	26.5 ± 6.5	29.4 ± 4.0	27.5 ± 4.1[a]	29.4 ± 4.6
$V^*_{m.space}$ (mm^3)	2.86 ± 1.4	3.05 ± 2.6	1.93 ± 0.57	2.34 ± 0.70	2.43 ± 1.3
$V^*_{b.space}$ (mm^3)	0.23 ± 0.08	0.28 ± 0.13	0.30 ± 0.18	0.36 ± 0.12	0.31 ± 0.16
Tb.Th (µm)	91.4 ± 9.0	99.7 ± 11	100 ± 15	104 ± 12	103 ± 12
Tb.N (mm^{-1})	2.78 ± 0.27	2.64 ± 0.44	2.94 ± 0.21	2.64 ± 0.16[b]	2.86 ± 0.21
Tb.Sp (µm)	271 ± 40	287 ± 80	242 ± 24	277 ± 30[a]	250 ± 33
Nd/Tm	0.93 ± 0.04	1.25 ± 0.70	1.22 ± 0.46	1.23 ± 0.49	0.97 ± 0.40
TBPf (mm^{-1})	–0.04 ± 1.1	0.20 ± 1.2	–0.30 ± 0.79	–0.40 ± 1.0	–0.18 ± 0.70

Table 1. Results are presented as means ± SD. [a] $p < 0.05$, [b] $p < 0.08$ compared with baseline.

The study has shown that 120 days of 5° head-down tilt bed rest without countermeasures resulted in a significant decrease of BV/TV and a significant increase of Tb.Sp. Furthermore, a decrease of Tb.N was also detected during 120 days of bed rest without countermeasures – but this was significant at the 0.08 level only. No other significant changes were found for the histomorphometric measures between any of the time points in either of the study groups. Finally, the combined treatment with bisphosphonate and exercise was able to prevent significant loss of bone during 370 days of antiorthostatic bed rest.

In contrast to the present study, Vico et al. found in subjects exposed to 120 days of 5° head-down tilt bed rest a non-significant decrease of iliac crest BV/TV of 1.2% [22], while Palle et al. found in subjects undergoing 120 days of 5° head-down tilt bed rest, a non-significant increase of iliac crest BV/TV of 2.8% [16]. However, they determined a significant loss of Tb.N after 120 days of bed rest, whereas in the present study this was significant at the 0.08 level only. Chappard et al. studied the effect of 120 days of 5° head-down tilt bed rest with and without bisphosphonate treatment and found that 120 days of bed rest induced a non-significant loss of iliac crest BV/TV of 13.5% without and 1.9% with countermeasures [2]. Zerwekh et al. found in normal subjects submitted to 84 days of horizontal bed rest a non-significant increase of iliac crest BV/TV of 7.5% [24]. However, they also determined non-significant decreases in lumbar spine BMD (2.9%) and femoral neck BMD (1.1%) and a significant decrease in the BMD of the greater trochanter (3.8%). LeBlanc et al. did not study the iliac crest *per se*, but found a significant loss of pelvic BMD of 4.9% when investigating six healthy men undergoing 119 days of horizontal bed rest [9]. The bone loss observed by LeBlanc et al. for the entire pelvic region (0.29% per week) is relatively close to what we have found in the present study for iliac crest bone biopsies (0.37% per week).

It is known from clinical studies that immobilization causes a very rapid loss of bone density. Hanson et al. thus showed a 2% loss of spinal bone density per week in patients during prolonged bed rest after scoliosis surgery [4], while Krølner and Toft found that simple bed rest of patients with backache due to protrusion of a lumbar intervertebral disc resulted in an average vertebral bone loss of 0.9% per week [8]. LeBlanc et al. showed that 5 weeks of bed rest resulted in a loss of spinal BMD of 0.21% per week [10], and in a later study that 17 weeks of horizontal bed rest resulted in a loss of lumbar spinal BMD of 0.34% per week [9]. In the present study, the loss of iliac crest bone volume (BV/TV) was 0.37% per week for the subjects exposed to 120 days of bed rest without countermeasures. The bone loss is thus less in healthy

subjects exposed to either horizontal or antiorthostatic bed rest than that found in the clinical studies by Hanson et al. [4] and Krølner and Toft [8].

Thomsen et al. have determined the relationship between BV/TV and age at the iliac crest for normal males and females [21]. Using these relationships, the relative age-related loss of BV/TV that takes place for males from 35 years to 36 years of age can be determined to 0.89% per year or 0.017% per week. The rate of bone loss induced by bed rest that was found in the present study is thus 22 times larger than what could be expected for similarly aged males not undergoing bed rest.

We found a very erratic pattern of behaviour of the two structural measures Nd/Tm and TBPf during bed rest without countermeasures. This inconsistent behaviour of these structural measures is probably due to the inhomogeneous distribution of the trabecular bone structure of the ileum, as the biopsies had to be obtained at different locations at the beginning of the study and at day 116.

The homogeneity of the trabecular bone structure of the iliac crest has previously been investigated [1,3,11,13]. These studies showed when two iliac crest bone biopsies were simultaneously obtained within a distance of 1–2 cm, reasonably close correlations could be established between histomorphometric measures derived from those two biopsies. However, if the distance between the biopsies was larger, the relationship between the histomorphometric measures from the two biopsies was substantially weaker. Likewise, some studies have also questioned the correlation between the histomorphometric properties of two biopsies obtained at the same location of the iliac crest at either side of the pelvis [17,23]. These studies usually considered BV/TV only, but it would be reasonable to assume that structural measures, such as Nd/Tm and TBPf, would be even more sensitive to biopsy location than BV/TV, which quantifies bone density rather than bone structure.

Since the structural properties of the iliac crest are not homogeneously distributed, observed differences in the bone structure may consequently reflect differences in the sampling site rather than differences between the two time points. Similarly, the lack of an observed difference might also be due to differences in the sampling site combined with the inhomogeneously distributed trabecular bone structure of the ileum. One way to decrease this measurement “noise” is to increase the number of test subjects substantially, which is neither feasible in bed rest studies nor in investigations conducted on space flying personnel. A further complicating factor in such studies is that the test subjects can only be recruited from a limited pool of individuals, which makes it difficult to create evenly balanced study groups.

This indicates that in longitudinal studies where only a few test subjects are available iliac crest bone biopsies is not the ideal tool for obtaining information about changes of the trabecular bone structure. It is probably prudent to consider whether a non-invasive radiological technique applied at a skeletal location, where it is possible to conduct repeated measurements of the same skeletal structure over time, would offer a better assessment of the structural trabecular bone status than iliac crest bone biopsies. In the first part of the project we suggested the proximal tibial metaphysis as such a skeletal location which is well suited for in vivo longitudinal assessment of the trabecular bone structure.

In the present study, we found that 120 days of antiorthostatic bed rest induced a loss of Tb.N, which was significant at the 0.08 level. We also found a concurrent non-significant increase in Tb.Th. Palle et al., who found a significant loss of Tb.N and a concomitant non-significant increase of Tb.Th, made a similar observation [16]. This may indicate that the thinnest trabeculae of the iliac network have been resorbed due to immobilization. When the thinnest trabe-

culae are removed the average thickness of the remaining trabeculae will increase, which can explain the simultaneous slight increase in trabecular thickness. However, in order to verify this conjecture a study with substantially more individuals needs to be carried out. Nevertheless, the results obtained in the present study as well as those obtained by Palle et al. indicate that the bed rest induced bone loss probably functions through a removal of thin trabeculae rather than through an overall thinning of the trabecular network. This is consistent with the recent study by Modlesky et al. that investigated the trabecular bone structure of the proximal tibial metaphysis of men with spinal cord injury and normal control subjects [12]. They found that BV/TV and Tb.N were decreased; Tb.Sp was increased; while Tb.Th was unchanged in the spinal cord-injured men compared with the normal controls. Furthermore, this is also consistent with the ability of the antiresorptive agent Xidifon, when given in combination with an exercise regimen, to prevent bone loss through trabecular perforations during the 370 days of antiorthostatic bed rest.

In conclusion: Bed rest without countermeasures results in a significant loss of bone density and in a significant altered bone structure at the iliac crest. There are non-significant indications that the bed rest induced bone loss involves removal of trabeculae without a general thinning of the trabeculae. A longitudinal series of iliac crest bone biopsies is not the ideal tool for investigating changes of the trabecular bone structure.

An article describing the results obtained through the study of the iliac crest bone sections from the bed rest study has been submitted for publication in Calcified Tissue International.

7.2 Biomechanical Test of the Vertebral Bodies

In order to evaluate the various structural measures ability to predict bone strength it is vital to determine the fracture strength of the examined bone. However, since both vertebral histomorphometry and biomechanics are destructive testing methods more than one vertebral body is required. Consequently, the third lumbar vertebral body (L3) was assigned for vertebral biomechanics, whereas the fourth lumbar vertebral body (L4) was assigned for vertebral histomorphometry.

Figure 12. Vertebra L3 with interface material placed in the materials testing machine.

Furthermore, we found that if the vertebral bodies were µCT scanned before and after the biomechanical testing, it would give us an opportunity to study the influence of the mechanical testing on the integrity of the trabecular bone structure. Therefore, it was vital that the vertebral bodies were tested intact. The problem with testing vertebral bodies intact is that the endplates are not plano-parallel. In order to make the endplates plane with the testing machine, without damaging the vertebral bodies, a two-component putty was identified as a potential interface material. Figure 12 shows a vertebral body with the putty in place on the vertebral endplates. The putty underwent a mechanical testing and it was found that the putty had a Young's modulus of approximately 20 MPa. This elasticity is very close to what have been found experimentally for canine lumbar intervertebral disci [25].

Before the vertebral bodies are tested, the volumes are determined by use of Archimedes' Principle. The heights of the vertebrae are determined by use of an electronic calliper. The average cross sectional area (CSA) is found as volume divided by vertebral height. Stress denotes applied force during compression normalized with the CSA, whereas strain denotes deformation normalized with vertebral height. The stress and strain values are thus size independent mechanical parameters which enable a comparison between vertebral bodies of different sizes.

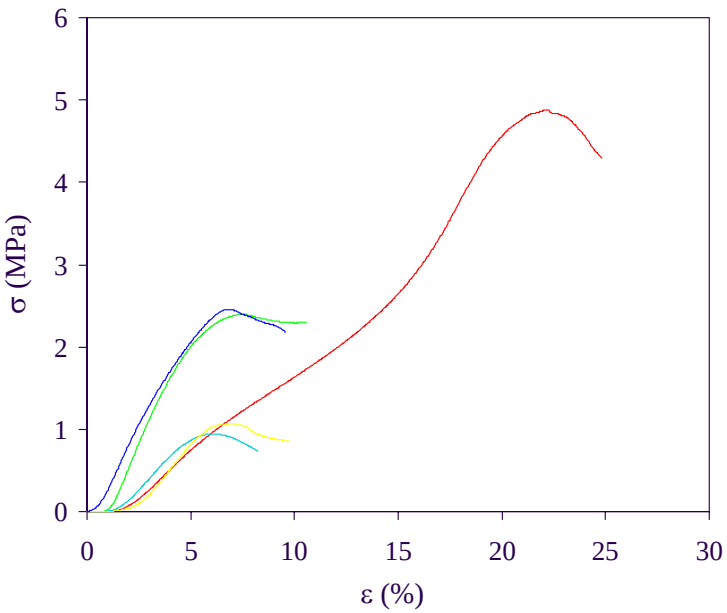

Figure 13. Stress-strain curves for five vertebrae.

Figure 13 shows the stress-strain curves obtained during compression of five vertebral bodies tested with the interface material in place. Due to the interface material being much more elastic that the vertebral bone the main part of the deformation takes place in the interface material during the compression testing. This means that the slope of the stress-strain curve quantifies Young's modulus of both the interface material and the bone. It is thus not possible, with the current set-up, to calculate the elasticity of the vertebral body alone.

However, due to the influence of formalin fixation on the elasticity of bone tissue we found that it was more essential to be able to µCT scan the vertebral bodies before and after the testing than to determine the elasticity. It is important to notice that the interface material does not influence the maximum stress value of the compression.

In conclusion: The proposed new method for testing vertebral bodies is a success. At the date of the report five vertebral bodies have been tested, while 20 vertebral bodies awaits the comparison of the "before" and "after" µCT scans of the five tested vertebral bodies (see Section 6) before the compression testing proceeds.

7.3 Histomorphometry of the Vertebral Bodies

Figure 14. The 9-mm-thick slice for histomorphometry is marked with red.

Static histomorphometry is performed as it is considered the "gold standard" for obtaining structural information of the trabecular bone network. In order to perform the best possible comparison between histomorphometry and the measures of complexity obtained by pQCT and CT the same region as evaluated by the CT techniques was selected for histomorphometry (Figure 14). However, as there is a limit to how large sections that can be handled and as the vertebral body to a large degree is left-right symmetrical only half of the vertebral cross section was used for histomorphometry (Figures 15). During the analysis of the pQCT images, it was established that the trabecular bone structure is not evenly distributed within the vertebral body. The region close to the posterior processes is much denser than the rest of the vertebral body (Figure 15). In the central posterior region large veins are exiting the vertebral body, which leads to a less dense bone network than found in the rest of the vertebra. Therefore, a region of interest (ROI) was created which excludes these areas (Figure 16A). The ROIs used during the pQCT analyses were traced onto the corresponding histological sections (Figure 16) in order to ensure maximal correspondence between the radiological and histological analyses.

Figure 15. Bone slice adjacent to that used for histomorphometry.

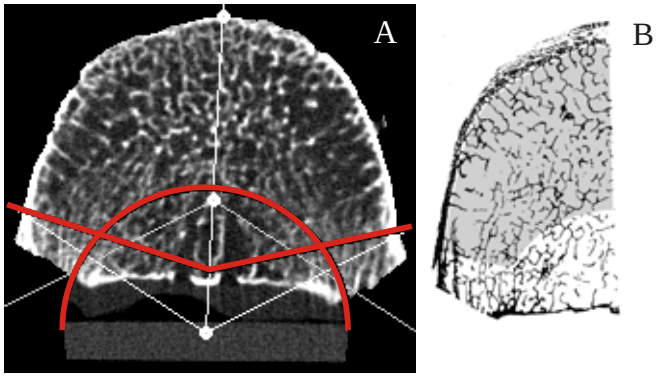

Figure 16. A: pQCT image with ROI superimposed. B: corresponding histological section with ROI superimposed.

The computer program used for the histomorphometric analyses is the same as used in the first phase of the project for the analysis of biopsies from the proximal tibial metaphysis.

Figure 17 show the vertebral bone strength plotted as a function of trabecular bone volume BV/TV for the five mechanically tested vertebral bodies. When all the histomorphometric measures are correlated with the compressive bone strength, BV/TV is the histomorphometric measure that correlates strongest with the bone strength. Therefore, even when the number of subjects is low, it is fair to conclude that trabecular bone volume is strongly correlated with

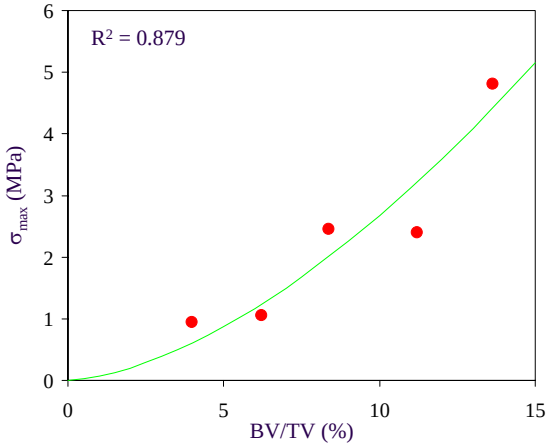

Figure 17 Maximum stress σ_{max} of L3 as a function of trabecular bone volume BV/TV of L4.

compressive bone strength. These findings are in accordance with previously published results for histomorphometry and compressive bone strength of vertebral bodies [20].

In conclusion: The applied methodology is working well and the histomorphometry proceeds without any problems. At the date of the report, histomorphometry has been finished on 14 of the 25 vertebral bodies.

8. Coordination and Cooperation between Team Members and Industry Partners

The team worked successfully together during the reported period January 2003–November 2004. The team members work in close contact with each other. The cooperation between the team members is excellent, as can be seen from the experimental part of this report and especially from the joined publications and contribution to the scientific meetings. The international cooperation between German, Danish, and Swiss partners as well as scientific cooperation with the Institute for Biomedical Problems (IBMP), Russia, and the Faculté de Médecine, Saint-Etienne, France, have already led to results which could not have be obtained if this project had been based on national resources alone.

The coordination between the academic teams and the industrial partners Scanco Medical AG, Siemens AG, and Mercury Computer Systems GmbH has been excellent. All three industrial partners contribute very valuable resources and services to this project. Without the contributions from the industrial partners this project would not have been possible.

Scanco Medical AG has provided its know-how, most up-to-date µCT-scanner and manpower for the needs of the project. Vertebral bodies were sent to Scanco and high-quality 3D µCT-data sets were received by the team (ZIB). In addition to the initially planned imaging, Scanco kindly agreed to additionally scan the third lumbar vertebrae after they were biomechanically tested. The coordinator, Peter Saparin (MPI), Gise Beller (CBF, responsible for preparation of the vertebral bodies) and Jesper Skovhus Thomsen (UoA, biomechanical tests and vertebral histomorphometry) are in telephone and e-mail contact with Scanco Medical (Bruno Koller and colleagues). The contribution by Scanco was very valuable to us as it made it possible to obtain high-quality 3D µCT-data sets acquired from an entire human lumbar vertebral body. The µCT system developed by Scanco is unique as it is currently the only system that makes this possible.

Siemens AG, Siemens Medical Solutions has been participating in the second phase of the project during almost two years and has supported the research by in kind donation of 50 k Euro per year as well as by participation in regular project meetings. Computed Tomography Division of Siemens (Klaus Klingenbeck-Regn, later Thomas von der Haar and Christian Asbeck) organized technical support of the experiments and data acquisition on CT-scanners available at CBF. As a part of their contribution to the project, Siemens delivered the promised financial part on time. The representatives from Siemens made valuable comments and suggestions to the research activities during project board meetings. In addition, the information and recommendations provided by Siemens's was very valuable to us in the interpretation of the results of our CT experiments and led to an optimization of the acquisition parameters for imaging of bone specimens and patients on the helical CT-scanners.

Cooperation with Scanco Medical AG and Siemens AG, Siemens Medical Solutions will continue in the future beyond the current project. In particular, both industry partners participate in new MAP-proposal submitted to ESTEC in November 2004 (see section 11.2).

Mercury Computer Systems GmbH, legal successor of Indeed – Visual Concepts GmbH, is providing the software framework Amira in which the specific visualization and analysis modules have been implemented. A new major version (Amira 3.1) was released in fall 2003. The industry partner provided software licences to the academic partners and supported the software development of the research group by providing consulting and by changing software interfaces in Amira according to needs of the project.

The achievements of this project could be enhanced by increased involvement of the pharmaceutical industry. Connections have been made resulting in a substantial financial contribution by **Roche Pharmaceuticals**. It can be envisioned that the association with Roche Pharmaceuticals will be important for further developments within a drug-based prevention program of bone loss under microgravity conditions.

9. Publications during the Time of the Report

1. P. Saparin, J.S. Thomsen, S. Prohaska, A. Zaikin, J. Kurths, H.-C. Hege, W. Gowin. Quantification of Spatial Structure of Human Proximal Tibial Bone Biopsies Using 3D Measures of Complexity. *Acta Astronautica*, 2004 (in press).

2. S. Prohaska, A. Hutanu, R. Kähler, H.-C. Hege. Interactive Exploration of Large Remote Micro-CT Scans. *Proc. IEEE Visualization '04*, pp. 345–352, Austin, Texas, 2004.

3. A. Zaikin, P. Saparin, J. Kurths, S. Prohaska, W. Gowin. Modelling Bone Resorption in 2D CT and 3D μCT Images. *Int. Journal of Bifurcation and Chaos*, 2004 (accepted for publication).

4. N. Marwan, P. Saparin, W. Gowin, J. Kurths. 3D Measures of Complexity for the Assessment of Complex Trabecular Bone Structures. *Proc. 2nd Meeting Complexity in the Living*, Rome, 2004 (in press).

5. J.S. Thomsen, A. Laib., B. Koller, S. Prohaska, Li. Mosekilde, W. Gowin. Stereological Measures of Trabecular Bone Structure: Comparison of 3D Micro Computed Tomography with 2D Histological Sections in Human Proximal Tibial Bone Biopsies. Submitted for publication in *Journal of Microscopy*. (Revised manuscript submitted 27 September 2004).

6. J.S. Thomsen, B.V. Morukov, L. Vico, C. Alexandre, P.I. Saparin, W. Gowin. The Effects of 370 Days of Antiorthostatic Bed Rest With and Without Countermeasures on Static Histomorphometry of Iliac Crest Bone Biopsies. Submitted for publication in *Calcified Tissue International*. (Submitted 16 November 2004).

7. P. Saparin, J. Kurths, W. Gowin. Segmentation of bone CT-images and assessment of bone structure using measures of complexity. *Medical Physics*. (revised manuscript to be resubmitted).

10. Contributions to Scientific Meetings

1. H.-C. Hege. Visualization in Biomedicine: Methods and Applications, *Summer School "Jacques Louis Lions" - Multidisciplinary Methods for Analysis, Optimization and Control of Complex Systems*, MACSI-net, Montecatini, Italy, March 17, 2003 **(oral presentation)**.

2. W. Gowin, P. Saparin, S. Beller, D. Felsenberg. Architectural reasons for the femoral neck fracture location. *2nd European Congress on Achievements in Space Medicine into Health Care Practice and Industry*, Berlin, Germany, March 27–29, 2003 (**oral presentation**).

3. S. Prohaska, H.-C. Hege, M. Giehl, W. Gowin, *Interactive Visualization to Support Quantitative Analysis of Bone Biopsies, 2nd European Congress on Achievements in Space Medicine into Health Care Practice and Industry*, Berlin, March 27–29, 2003 (**oral presentation)**

4. P. Saparin, W. Gowin, A. Zaikin, S. Prohaska. Quantification of changes in human bone structure at different skeletal locations using measures of complexity. *2nd European Congress on Achievements in Space Medicine into Health Care Practice and Industry*, Berlin, Germany, March 27–29, 2003 (**oral presentation**).

5. J.S. Thomsen, B. Koller B, A. Laib, S. Prohaska, M. Giehl, W. Gowin. Comparison between static histomorphometric measures conducted by traditionally 2D histomorphometry and 3D µ-CT in human tibial biopsies. *2nd European Congress on Achievements in Space Medicine into Health Care Practice and Industry*, Berlin, Germany, March 27–29, 2003 (**oral presentation**).

6. A. Zaikin, P. Saparin, S. Prohaska, J. Kurths, W. Gowin. 2D and 3D bone modelling for analysis of changes in the bone architecture and for evaluation of structural measures. *2nd European Congress on Achievements in Space Medicine into Health Care Practice and Industry*, Berlin, Germany, March 27–29, 2003 (**oral presentation**).

7. H.-C. Hege: Creation and Visualization of 3D Anatomical Models, *3D Modelling 2003*, Paris, April 23, 2003 **(oral presentation).**

8. H.-C. Hege: From 3D Image Data to 3D Geometrical Models, *Seminar "Numerische Mathematik und Wissenschaftliches Rechnen"*, Universität Duisburg, FB Mathematik, May 15, 2003 **(oral presentation)**.

9. W. Gowin, P. Saparin. Skeletal locations for the examination of bone structure alterations due to microgravity exposure. *14th IAA Humans in Space Symposium*, Banff, Alberta, Canada, May 18–22, 2003 (**oral presentation**).

10. P. Saparin, W. Gowin, A. Zaikin, J.S. Thomsen, S. Prohaska, H.-C. Hege, J. Kurths. Quantification of spatial structure of human proximal tibial bone biopsies using 3D measures of complexity. *14th IAA Humans in Space Symposium*, Banff, Alberta, Canada, May 18–22, 2003 (**oral presentation**).

11. S. Prohaska, H.-C. Hege, M. Giehl, W. Gowin. A virtual laboratory for assessment of bone biopsies. *14th IAA Humans in Space Symposium*, Banff, Alberta, Canada, May 18–22, 2003 (**oral presentation**).

12. H.-C. Hege: Creating 3D Geometrical Models from 3D Image Data, *Tandem Workshop "Geometry, Numerics and Visualization"*, Sauen, DFG Research Center Matheon "Mathematics for Key Technologies", May 26, 2003 **(oral presentation)**.

13. H.-C. Hege: Perceptually Effective 3D Visualization of Complex Data, *2003 Computer Graphics and Visualization Festa*, Nikkei Science, Tokyo, Japan, October 4, 2003 **(keynote lecture)**.

14. H.-C. Hege: Datenanalyse - numerische Extraktion von geometrischen und topologischen Merkmalen, *Physikalisch-Technische Bundesanstalt (PTB)*, Berlin, March 18, 2004 **(oral presentation)**.

15. P. Saparin on behalf of the project team. 3D Quantification of bone structure and its changes in microgravity condition by measures of complexity. *DLR Human Physiology Workshop*, Cologne, Germany, May 13–14, 2004 (**oral presentation**).

16. S. Prohaska. Exploring high-resolution medical image data. *BIRS Workshop on Mathematical Foundations of Scientific Visualization, Computer Graphics, and Massive Data Exploration*, Banff, Alberta, Canada. May 22–27, 2004 (**oral presentation**).

17. H.-C. Hege: Moderne Visualisierung - versteckte Zusammenhänge sichtbar machen, TU Darmstadt, *Mathematisches Kolloquium*, May 26, 2004 **(oral presentation)**

18. G. Beller, P. Saparin, W. Gowin. Structural measures of complexity in pQCT- and helical-CT-imaging. *International workshop on Musculoskeletal and Neuronal Interactions*, Chalkidiki, Greece, May 28–31, 2004, (**poster presentation**).

19. W. Gowin, P. Saparin, J.S. Thomsen, S. Prohaska, H.-C. Hege. The proximal tibia: A new site for bone status assessments. *25th Annual International Gravitational Physiological Meeting*, Moscow, Russia, June 6–11, 2004 (**oral presentation**).

20. P. Saparin, J. S. Thomsen, S. Beller, G. Beller, W. Gowin. Comparison of pQCT image analysis and histomorphometry to quantify bone structural loss in the proximal tibia. *25th Annual International Gravitational Physiological Meeting*, Moscow, Russia, June 6–11, 2004 (**oral presentation**).

21. J.S. Thomsen, B.V. Morukov, L. Vico, P.I. Saparin, W. Gowin. Static histomorphometry of the iliac crest after 360 days of antiorthostatic bed rest with and without countermeasures. *25th Annual International Gravitational Physiological Meeting*, Moscow, Russia, June 6–11, 2004 (**oral presentation**).

22. N. Marwan, P. Saparin, W. Gowin, J. Kurths. On the way to new 3D measures of complexity for bone assessment. *8th Experimental Chaos Conference*, Florence, June 14–17, 2004 (**poster presentation**).

23. J.S. Thomsen, B.V. Morukov, L. Vico, P.I. Saparin, W. Gowin. Static histomorphometry of the iliac crest after 360 days of antiorthostatic bed rest with and without

countermeasures. *35th COSPAR (Committee on Space Research) Scientific Assembly*, Paris, France, July 18–25, 2004 (**oral presentation**).

24. N. Marwan, P. Saparin, W. Gowin, J. Kurths. 3D measures of complexity for the assessment of trabecular bone structures. *2-nd International Meeting "Complexity in the Living"*, Rome, Italy, September 28–30, 2004 (o**ral presentation and poster**).

25. S. Prohaska. Interactive exploration of large remote micro-CT scans. *IEEE Visualization 2004*. Austin, Texas, USA. October 10–15, 2004 (**oral presentation**).

26. J. Kurths, N. Marwan, P. Saparin, S. Prohaska, W. Gowin. Quantification of human bone measurements using measures of complexity. *Ollendorff Minerva Center for Vision and Image Sciences German-Israeli Binational Workshop*, Haifa, October 20–21, 2004 (**invited oral presentation**).

27. H.-C. Hege: SciVis Cooperation between LSU & ZIB: Potential Research Goals, Louisiana State University, Center for Computation and Technology, Baton Rouge, Louisiana, USA, Oct. 18, 2004 **(oral presentation)**.

28. S. Prohaska. Interactive visual data analysis of terrascale data: an achievable goal? *CCT Seminar*, Baton Rouge, Louisiana, USA, October 26, 2004 (**oral presentation**).

29. H.-C. Hege: Distributed Visualization and Data Analysis, *Visualization Workshop*, Kanazawa University, Kanazawa, Japan, Nov 15, 2004 **(oral presentation).**

11. Brief Review of Activities for the Second Part of the Project

11.1 Activities to be completed in the project

Study of bone structure and its alteration with 2D measures of complexity:

- Continuous examination of patients by applying the developed technique of bone structural evaluation with 2D measures of complexity to different skeletal sites: lumbar vertebrae and proximal tibia. The examinations of patients and bone structural alterations during follow-up measurements are planed to take place at the CBF as an additional part of an ADOC study. Up to 6 patients that have become paralyzed (hemiplegic or paraplegic) after a stroke will be examined during a follow up period of 6 month for the study. From all patients CT-images of lumbar vertebrae and both left and right proximal tibiae will be collected at baseline (trauma), and again 3 and 6 months after baseline. Moreover, the developed approach is also ready to be applied to astronauts' data if available.

Further development and refinement of 3D visualization tools, 3D preprocessing, 3D measures of complexity:

- We will concentrate our research on further refinement of the complexity measures based on iso-surface constructed with the marching cubes algorithm, local curvature, and orientation of trabeculae. In addition, the focus will be on measures derived from different moving window sizes. Moreover, the relationship between the marching cubes configurations and the local curvatures will be explicitly used for this refinement. Sensitivity and efficiency of the proposed 3D measures will be tested for complex 3D trabecular bone

structures of proximal tibiae and lumbar vertebrae as well as for artificial 3D test models. The 3D measures will be optimized with respect to their efficiency and computational requirements.

- Amira's 3D visualization and data processing tools will be further developed and expanded. Improving the capabilities of handling data sets that is larger than the main memory is the major focus. An efficiently workflow for analyzing the µCT scans of vertebral bodies will be established.
- Tools for visual and geometrically based 3D statistical assessment of structural changes will be available as Amira modules or Amira script objects. Within the Amira framework, a complete working environment will be established integrating 3D image analysis, geometry reconstruction, visualization, 3D measurement, and simulation procedures.
- Preliminary assessment about the ability to evaluate quantitatively the changes in the 3D bone structure after exposure to microgravity can be made, provided the project has access to bone imaging data from space-flying personnel.

Further development of bone models and their testing in 2D and 3D:

- Model studies will be adapted to bone imaging modalities. Using the model for data evaluation, we will study typical 3D bone architecture and its changes during the bone loss using measures of complexity to evaluate both the models and the developed structural measures. The model developed at MPI (see materials of Mid-Term Meeting) will be applied to the data from proximal tibiae and lumbar vertebrae. The results of the simulation will be evaluated with the structural measures being developed.
- Development of models that will provide insight into bone deterioration and that will be able to predict certain behaviours under continuous disuse, unloading, and remodeling conditions.

Finalization of the quantitative assessment of vertebral specimens based on µCT, histomorphometry, biomechanical tests, and 3D measures of complexity:

- Histomorphometry will be preformed and finished as planned with the method we have successfully developed.
- All remaining vertebrae will be biomechanically tested using the methodology that is described in this report.
- All remaining vertebral bodies will be scanned with µCT after undergoing biomechanical testing. The procedure has been established as reported in this document.
- Final evaluation of structural measures of complexity based on failure load assessment of lumbar vertebral specimens.
- Qualified statement about the quantitative assessment of lumbar vertebrae of patients based on new CT-technology.

The results of **bone structure assessment with ultrasound** will be compared with the results provided by the developed approaches, provided that we successfully bring a new ultrasound partner into the project. The calcaneal specimens for such a comparison have already been harvested and prepared at CBF.

Synopsis and synthesis of 2D and 3D imaging data will be performed. When the results of the planned research are available, a thorough evaluation and conclusion will be made as to which examination procedure will be able to deliver the most precise results for a bone status assessment. This will provide an ability to evaluate quantitatively the changes in the 2D and 3D bone structure after exposure to microgravity and during osteoporotic bone changes in patients on Earth.

11.2 Beyond the project

After the end of the current project the developed approach to quantify 3D bone structure with measures of complexity will be used to evaluate 3D data of astronauts which will be available from EDOS study, as agreed with ESTEC (Dr. Roger Binot) and EDOS coordinating team. 3D images of distal radius before and after the space flight will be acquired on an *in-vivo* µCT scanner manufactured by our project partner Scanco Medical AG.

In addition to the scientific task listed above, the project team has submitted a new proposal ESA-AO-2004-PCP-125 "Assessing the influence of microarchitecture on the mechanical performance of bone and its changes in microgravity from in-vivo measurements", which will logically continue the current research bringing it to a new level of understanding the relation between the bone architecture and its mechanical properties. Our main industry partners Scanco Medical AG and Siemens AG, Siemens Medical Solutions participate in new proposal.

12. References

1. Bordier P, Matrajt H, Miravet L, Hioco D. Mesure histologique de la masse et de la résorption des travées osseuses. Pathol Biol 12:1238–1243; 1964.
2. Chappard D, Alexandre C, Palle S, Vico L, Morukov BV, Rodionova SS, Minaire P, Riffat G. Effects of a bisphosphonate (1-hydroxy ethylidene-1,1 bisphosphonic acid) on osteoclast number during prolonged bed rest in healthy humans. Metabolism 38:822–825; 1989.
3. Ellis HA, Peart KM. Quantitative observations on mineralized and non-mineralized bone in the iliac crest. J Clin Pathol 25:277–286; 1972.
4. Hansson TH, Roos BO, Nachemson A. Development of osteopenia in the fourth lumbar vertebra during prolonged bed rest after operation for scoliosis. Acta Orthop Scand 46:621–630; 1975.
5. Kakurin LI, Kuzmin MP, Matsnev EI, Mikhailov VM. Physiological effects induced by antiorthostatic hypokinesia. Life Sci Space Res 14:101–108; 1976.
6. Kakurin LI, Lobachik VI, Mikhailov VM, Senkevich YA. Antiorthostatic hypokinesia as a method of weightlessness simulation. Aviat Space Environ Med 47: 1083–1086; 1976.
7. Krupina TN, Fyodorov BM, Filatova LM, Tsyganova NI, Matsnev EI. Effect of antiorthostatic bed rest on the human body. Life Sci Space Res 14:285–287; 1976.
8. Krølner B, Toft B. Vertebral bone loss: an unheeded side effect of therapeutic bed rest. Clin Sci 64:537–540; 1983.
9. LeBlanc AD, Schneider VS, Evans HJ, Engelbretson DA, Krebs JM. Bone mineral loss and recovery after 17 weeks of bed rest. J Bone Miner Res 5:843–850; 1990.
10. LeBlanc A, Schneider V, Krebs J, Evans H, Jhingran S, Johnson P. Spinal bone mineral after 5 weeks of bed rest. Calcif Tissue Int 41:259–261; 1987.
11. Melsen F, Melsen B, Mosekilde Le. An evaluation of the quantitative parameters applied in bone histology. Acta Pathol Microbiol Scand A 86:63–69; 1978.
12. Modlesky CM, Majumdar S, Narasimhan A, Dudley GA. Trabecular bone microarchitecture is deteriorated in men with spinal cord injury. J Bone Miner Res 19:48–55; 2004.
13. Moore RJ, Durbridge TC, Woods AE, Vernon-Roberts B. Variation in histomorphometric estimates across different sites of the iliac crest. J Clin Pathol 42: 814–816; 1989.
14. Nazarian A, Müller R. Time-lapsed microstructural imaging of bone failure behaviour. J Biomech 37: 55–65; 2004.
15. Odgaard A, Gundersen HJG. Quantification of connectivity in cancellous bone, with special emphasis on 3-D reconstructions. Bone 14:173–182; 1993.
16. Palle S, Vico L, Bourrin S, Alexandre C. Bone tissue response to four-month antiorthostatic bedrest: A bone histomorphometric study. Calcif Tissue Int 51:189–194; 1992.
17. Parisien MV, McMahon D, Pushparaj N, Dempster DW. Trabecular architecture in iliac crest bone biopsies: Infra-individual variability in structural parameters and changes with age. Bone 9:289–295; 1988.
18. Stepantsov VI, Eremin AV, Tikhonov MA. Means and methods of human physical training during long term space flight. In: Parin VV (ed) Weightlessness. Medicina, Moscow, Russia, pp 298–314; 1985.

19. Thomsen JS, Ebbesen EN, Mosekilde Li. A new method of comprehensive static histomorphometry applied on human lumbar vertebral cancellous bone. Bone 27:129–138; 2000.
20. Thomsen JS, Ebbesen EN, Mosekilde Li. Predicting human vertebral bone strength by vertebral static histomorphometry. Bone 30:502–508; 2002.
21. Thomsen JS, Ebbesen EN, Mosekilde Li. Relationships between static histomorphometry and bone strength measurements in human iliac crest bone biopsies. Bone 22:153–163; 1998.
22. Vico L, Chappard D, Alexandre C, Palle S, Minaire P, Riffat G, Morukov B, Rakhmanov S. Effects of a 120 day period of bed-rest on bone mass and bone cell activities in man: Attempts at countermeasure. Bone Miner 2:383–394; 1987.
23. Visser WJ, Roelofs JMM, Duursma SA. Bone density in the iliac crest. Metab Bone Dis Relat Res 3:187–190; 1981.
24. Zerwekh JE, Ruml LA, Gottschalk F, Pak CYC. The effects of twelve weeks of bed rest on bone histology, biochemical markers of bone turnover, and calcium homeostasis in eleven normal subjects. J Bone Miner Res 13:1594–1601; 1998.
25. Zimmerman MC, Vuono-Hawkins M, Parsons JR, Carter FM, Gutteling E, Lee CK, Langrana NA. The mechanical properties of the canine lumbar disc and motion segment. Spine 17:213–220; 1992.